Theoretical investigations on elastic properties, phase stability, and magnetism in Ni_2Mn-based all-d-metal Heusler compounds

Guijiang Li [1,*] Enke Liu [2,3,†] Wenhong Wang,[2,3] and Guangheng Wu[2]

[1]*College of Materials Science and Engineering, Nanjing Tech University, Nanjing 211816, People's Republic of China*
[2]*State Key Laboratory for Magnetism, Institute of Physics, Chinese Academy of Sciences, Beijing 100190, China*
[3]*Songshan Lake Materials Laboratory, Dongguan, Guangdong 523808, China*

(Received 27 January 2022; revised 15 February 2023; accepted 30 March 2023; published 28 April 2023)

The elastic properties, phase stability, and magnetism and correlations among them in all-d-metal Heusler compounds, i.e., Ni_2MnT (T = Sc, Ti, V, Cr, Y, Zr, Nb, Mo, Hf, Ta, and W) were systematically investigated by first-principles calculations. The results indicated that Ni_2MnT compounds were not fully consistent with the conventional atomic preferential occupation rule in the Heusler family. Within the scope of Heusler structures, Ni_2MnT compounds containing early transition metal atoms preferred $L2_1$-type structure, while those with late transition metal atoms were relatively stable in Hg_2CuTi-type structure. In d-d interatomic hybridization-controlled all-d-metal Ni_2MnT Heusler compounds, the atomic radius determined the lattice sizes. Owing to the strong couplings among elastic parameters, phonon modes, and electronic structure, the most likely martensitic phase transition could be expected in weakly magnetic Ni_2MnT compounds with late transition metal atoms. By applying hydrostatic pressure or imposing chemical pressure via adjusting the composition of Ti in an off-stoichiometric Ni-Mn-Ti system, magnetism was weakened, and the suppressed martensitic phase transition could be re-evoked. In this paper, we also revealed that experimentally observed antiferromagnetism in Ni_2MnTi originated from the arrest of the atomic diffusion process during the transition from the high-temperature chemically disordered paramagnetic state to the low-temperature chemically and magnetically ordered ferromagnetic state, which resulted in the formation of an intermediate metastable and partially disordered antiferromagnetic phase. Comparatively, Ni_2MnT compounds with early transition metals showed better ductility. In representative Ni_2MnY and Ni_2MnTa, it was found that nondirectional d-d interatomic hybridization became prevailing and helped establish the metal bonding character, which consequently enhanced the ductility. This paper can provide more insight into understanding the mechanism of martensitic phase transition and the origin of experimental anomalous magnetic states as well as the scheme to design multiple functional magnetic materials with outstanding ductility in the all-d-metal Heusler family. Experimentally observed exceptional multicaloric effects in Ni-Mn-based compounds with outstanding mechanical properties make all-d-metal Heusler compounds attractive for potential solid-state refrigeration application.

DOI: 10.1103/PhysRevB.107.134440

I. INTRODUCTION

Energy-efficient and environment-friendly solid-state refrigeration is the most promising alternative to the conventional vapor-compression cooling technology, and the essential prerequisites to successfully achieve solid-state refrigeration include high-performance phase transition materials with high cooling capacity. These materials possess outstanding phase transition characteristics so that they can produce large isothermal entropy change and adiabatic temperature change, which are ideal for high-efficiency cooling devices [1–8]. Among this type of materials, the Heusler family constitutes the most promising candidate materials. Their rich candidate material system, tunable phase transition temperature and hysteresis, quick response to multiple fields, and higher multiple-caloric effects make Heusler compounds more attractive from the perspective of not only industrial application but also fundamental research [7,8]. The other side of conventional Heusler compounds includes their inherent brittleness due to the strong p-d covalent hybridization between the first-nearest-neighbor (1nn) atomic pairs of transition metal atoms and main group elements [9–14]. The poor ductility degrades the fatigue life and service ability, posing the biggest challenges for their utilization as solid-state refrigerant materials. To the greatest possibility of maintaining their functionalities, concrete and strenuous efforts have been devoted to improve their ductility by introducing the second phase [9,10], strengthening the grain boundary [11,12], and microalloying the rare earth elements [13,14]. Owing to the lack of fundamentally changing p-d covalent hybridization-dominated atomic bonding, the improvement of ductility is limited. Thus, systematic exploration of the phase transition materials with outstanding ductile properties is imperative.

Apart from the p-d covalent hybridization between different p- and d-group elements in the Heusler family, the d-d hybridization between different d-group elements also

*guijiangli@njtech.edu.cn
†ekliu@iphy.ac.cn

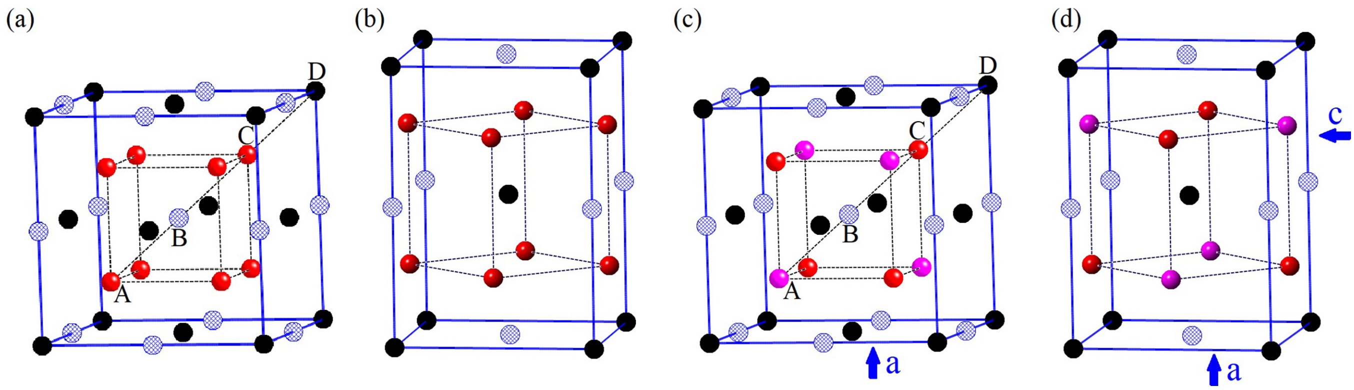

FIG. 1. (a) Regular cubic Heusler structure, i.e., $L2_1$-type or Cu_2MnAl-type structure (space group $Fm\bar{3}m$, No. 225). (b) Regular tetragonal Heusler structure (space group *I*4/*mmm*, No. 139). (c) Inverse cubic Heusler structure, i.e., Hg_2CuTi-type structure (space group $F\bar{4}3m$, No. 216). (d) Inverse tetragonal Heusler structure (space group $I\bar{4}m2$, No. 119). In cubic structure, A, B, C, and D represent four interpenetrating face-centered cubic (fcc) sublattices, whose Wyckoff coordinates are (0 0 0), ($\frac{1}{4}$ $\frac{1}{4}$ $\frac{1}{4}$), ($\frac{1}{2}$ $\frac{1}{2}$ $\frac{1}{2}$), and ($\frac{3}{4}$ $\frac{3}{4}$ $\frac{3}{4}$), respectively.

to some extent contributed to the formation and stabilization of Heusler phases [15]. Based on this, Wei *et al.* [15,16] experimentally realized that the Heusler phase could be formed without the *p*-group elements. They classified this type of material as all-*d*-metal Heusler compounds, which enriched the category of the Heusler family and expanded its research field. Recently, the concept of all-*d*-metal Heusler compounds has been well established [17]. Experimentally, all-*d*-metal Heusler compounds with typical phase transition exhibit improved mechanical properties. Owing to the good mechanical properties and large volume change observed across phase transition, the colossal elastocaloric effect under an applied stress of 700 MPa [18] and the giant barocaloric effect at 4 kbar [19] were experimentally achieved in polycrystalline all-*d*-metal Ni-Mn-Ti shape memory compounds. Moreover, in directionally solidified all-*d*-metal Heusler metamagnetic shape memory compounds, the martensitic transformation was found to be sensitive to applied pressure and stress. Low pressure-induced giant barocaloric effect [20] and large elastocaloric effect under a low critical stress [21] were observed in directionally solidified Ni-Co-Mn-Ti compounds. Moreover, mechanically and chemically stable Ni-Co-Mn-Ti rapidly solidified ribbons and quenched samples exhibited giant enhancement of the magnetocaloric response for a moderate field change of 2 T [22,23]. It is comparable with or larger than those of the best-known materials for near-room-temperature applications. Furthermore, due to the strong magnetostructural coupling in Ni-Mn-Ti-based compounds, their martensitic phase transition temperature and entropy changes can be jointly tailored by applying a magnetic field and hydrostatic pressure. When the magnetic field and hydrostatic pressure are applied in a proper sequence, the reversible entropy change gets effectively enhanced [20,24]. All the abovementioned advantages make Ni-Mn-based all-*d*-metal Heusler compounds popular for the design and exploration of multicaloric materials for solid-state refrigeration application. Detailed comparisons are shown in the Supplemental Material [25] (see also Refs. [5,8,11,12,18–22,26–59] therein). However, current experiments mainly concentrate on the Ni-Mn-Ti system and its derivative [15,16,18–24,60,61]. Thus, identification of more outstanding all-*d*-metal Heusler compounds that can serve as potential solid-state refrigeration materials is important. Currently, despite the potential importance of all-*d*-metal Heusler compounds for solid-state refrigeration application, fully fundamental understanding about the mechanism of martensitic phase transition and anomalous magnetic behavior as well as improved ductility is still lacking.

In this paper, elastic properties, phase stability, and magnetism and correlations among them in all-*d*-metal Ni_2MnT (T = Sc, Ti, V, Cr, Y, Zr, Nb, Mo, Hf, Ta, and W) Heusler compounds were systematically investigated by first-principles calculations. Furthermore, the mechanism of martensitic phase transition, origin of experimental anomalous magnetic states, and improved ductility are comprehensively discussed. It is believed that this paper can help explore more excellent phase transition materials for solid-state refrigeration, with outstanding mechanical properties from both experimental and theoretical perspectives.

II. CALCULATION METHODS

Like those in conventional Ni-Mn-based full Heusler compounds, two possible high-ordered cubic structures, i.e., $L2_1$- and Hg_2CuTi-type structures, were considered herein for Ni_2MnT compounds. They are shown in Figs. 1(a) and 1(c), respectively. First, the specific structure was determined for Ni_2MnT compounds. Then based on the obtained structures, the first-principles calculations were performed.

In this paper, structure information, elastic parameters, electronic structure, phonon dispersions, and magnetism of Ni_2MnT compounds were investigated by first-principles calculations. When computing the total energy, the adoption of the full charge density via the exact muffin-tin orbitals (EMTO) method not only improves the calculation efficiency but also leads to high accuracy [62]. Thus, the theoretical calculations were performed mainly by the EMTO method. Moreover, random occupation of atoms in off-stoichiometric Heusler compounds was investigated by using the coherent potential approximation (CPA) [63–65].

Previously, numerous studies have verified its feasibility on alloys and compounds [18,66–70]. The EMTO basis sets included s, p, d, and f orbitals. The muffin-tin potential parameters, i.e., the radius of the muffin-tin potential sphere of the Ni site ($R_{\mathrm{mt}}^{\mathrm{Ni}}$) and the atomic radius of the Ni site ($R_{\mathrm{ws}}^{\mathrm{Ni}}$), were selected as $R_{\mathrm{mt}}^{\mathrm{Ni}} = 0.95R_{\mathrm{ws}}$ and $R_{\mathrm{ws}}^{\mathrm{Ni}} = 1.10R_{\mathrm{ws}}$, where R_{ws} is the average Wigner-Seitz radius [71–73]. For the other sublattices, a default setup $R_{\mathrm{mt}} = R_{\mathrm{ws}}$ was adopted. The soft-core approximation was employed. The Ni $3d^8\,4s^2$, Mn $3d^5\,4s^2$, Sc $3d^1\,4s^2$, Ti $3d^2\,4s^2$, V $3d^3\,4s^2$, Cr $3d^4\,4s^2$, Y $4d^1\,5s^2$, Zr $4d^2\,5s^2$, Nb $4d^3\,5s^2$, Mo $4d^4\,5s^2$, Hf $5d^2\,6s^2$, Ta $5d^3\,6s^2$, and W $5d^4\,6s^2$ states were treated as the valence electron states. The paramagnetic (PM) state was described by using the disordered local moment approach [74,75]. The density of states (DOS) was calculated by adopting the integration method of interpolation. The electron localization function (ELF) and phonon properties (with the method of finite displacement) were calculated directly by the pseudopotential method implemented in the CASTEP code. The size of the supercell was 27 times that of the primitive cell used in the calculation of the phonon properties. The energy convergence criterion and density plane-wave cutoff were set to 1×10^{-6} eV atom^{-1} and 500 eV, respectively. The ultrasoft pseudopotential was selected to describe the interactions between the atomic core and the valence electrons [76]. A Monkhorst-Pack phonon q-vector grid of $8 \times 8 \times 8$ was adopted for the calculation of phonon dispersions and phonon DOSs. During all calculations, the exchange-correlation energy of electrons was solved by using GGA-PBE [77]. A Monkhorst-Pack k-point grid of $15 \times 15 \times 15$ was used for the electronic properties.

The elastic properties of cubic all-d-metal Heusler compounds can be fully described by using three independent elastic constants, i.e., C_{11}, C_{12}, and C_{44}. The C_{11} and C_{12} were obtained from the tetragonal shear modulus $C' = (C_{11} - C_{12})/2$ and the bulk modulus $B = (C_{11} + 2C_{12})/3$ [62]. In this paper, the equilibrium volume and bulk modulus were determined by fitting the calculated total energy vs volume to a Morse function [78]. The tetragonal shear modulus C' and the cubic elastic modulus C_{44} were derived from the volume-conserving orthorhombic deformation and monoclinic deformation, namely, $\begin{pmatrix} 1+\delta_o & 0 & 0 \\ 0 & 1-\delta_o & 0 \\ 0 & 0 & \frac{1}{1-\delta_o^2} \end{pmatrix}$ and $\begin{pmatrix} 1 & \delta_m & 0 \\ \delta_m & 1 & 0 \\ 0 & 0 & \frac{1}{1-\delta_m^2} \end{pmatrix}$, respectively. Six distortions $\delta = 0.00, 0.01, \ldots, 0.05$ were adopted to calculate the total energies $E(\delta_o)$ and $E(\delta_m)$. By fitting the total energies with respect to δ_o and δ_m as $E(\delta_o) = E(0) + 2VC'\delta_o^2$ and $E(\delta_m) = E(0) + 2VC_{44}\delta_m^2$, C' and C_{44} were obtained. By these methods, the three elastic constants C_{11}, C_{12} and C_{44} can be determined.

The calculated structure information in Sec. III A, elastic related parameters in Sec. III B, electronic structures in Sec. III C, and magnetic moment in Sec. III E by the EMTO method can be compared with available values calculated by CASTEP and other methods. This consistency provides a prerequisite for the reasonable combination of the CASTEP method to discuss trends in chemical bonding by ELF in Sec. III B and describe phase stability by phonon properties in Secs. III D and III E. The effectively combination of these two methods can help us deeply understand the mechanism of martensitic phase transition and enhanced ductility in Ni_2Mn-based all-d-metal Heusler compounds.

III. RESULTS AND DISCUSSION

A. Structure information at the ground states

The conventional full Heusler compounds with the general formula X_2YZ can crystallize into $L2_1$- or Hg_2CuTi-type structures. Based on available knowledge and findings about all-d-metal Heusler compounds, these two possible crystal structures were considered herein to investigate the ground state properties. The calculated structural information of all-d-metal Ni_2MnT Heusler compounds is presented in Fig. 2. In this paper, the relative stability of Ni_2MnT compounds within the scope of Heusler structures was determined by the energy difference ΔE between the $L2_1$- and Hg_2CuTi-type structures. The positive ΔE indicates that the Hg_2CuTi-type structure is relatively stable compared with the $L2_1$-type structure. Otherwise, the $L2_1$-type structure is relatively stable. First, Fig. 2(a) illustrates that Ni_2MnT compounds containing late transition metals V, Cr, Mo, and W show positive ΔE. However, the ΔE values for Ni_2MnT compounds with early transition metals on the left of periodic table are all negative. It indicates that, like conventional Ni_2MnGa, Ni_2MnT (T = Sc, Ti, Y, Zr, Nb, Hf, and Ta) compounds preferentially remain in $L2_1$-type structures. Although Ni_2MnT (V, Cr, Mo, and W) compounds consist of similar constituent atoms, they are relatively stable in the Hg_2CuTi-type structure. The two Ni atoms occupy the A and B sites of the Hg_2CuTi-type structure. Moreover, Mn and the late transition metal atoms (V, Cr, Mo, and W) reside in C and D sites, respectively. This atomic configuration behavior disobeys the generalized adopted preferential occupation rule for atoms in conventional Heusler compounds [83]. Similar atomic occupation behavior was also observed in other V-based all-d-metal Heusler compounds [80,82]. It is thus speculated that this anomalous atomic configuration in all-d-metal Heusler compounds can bring out unique properties.

The cohesive energy is an important magnitude to predict the viability of experimental synthesis of Ni_2MnT compounds [84,85]. Theoretically, the cohesive energy of Ni_2MnT (T = Sc, Ti, V, Cr, Y, Zr, Nb, Mo, Hf, Ta, and W) compounds in this paper can be obtained by using $E_{\mathrm{coh}} = (E_{\mathrm{Ni}}^{\mathrm{iso}} + E_{\mathrm{Mn}}^{\mathrm{iso}} + E_{T}^{\mathrm{iso}}) - E_{\mathrm{Ni_2Mn}T}^{\mathrm{Total}}$, where $E_{\mathrm{Ni}}^{\mathrm{iso}}$, $E_{\mathrm{Mn}}^{\mathrm{iso}}$, and E_{T}^{iso} are isolated atomic energy of Ni, Mn, and T atoms, respectively, and $E_{\mathrm{Ni_2Mn}T}^{\mathrm{Total}}$ denotes the total energy of Ni_2MnT. To characterize the possibility of experimental synthesis of Ni_2MnT compounds within their specific Heusler structures, the cohesive energies were calculated in this paper and are shown in Fig. 2(b). The cohesive energy of Ni_2MnTi is 21.14 eV/f.u. It has been successfully prepared experimentally in the Heusler-type structure [15]. For well-known Ni_2MnGa, the calculated cohesive energy is 17.64 eV/f.u. It was also experimentally prepared in the Heusler-type structure [86]. For other Ni_2MnT compounds, their cohesive energy ranges from 17.06 to 21.82 eV/f.u. Theoretically, they can be compared with values of both Ni_2MnTi and Ni_2MnGa. Thus, Ni_2MnT compounds in this paper may be experimentally synthesized at their specific Heusler

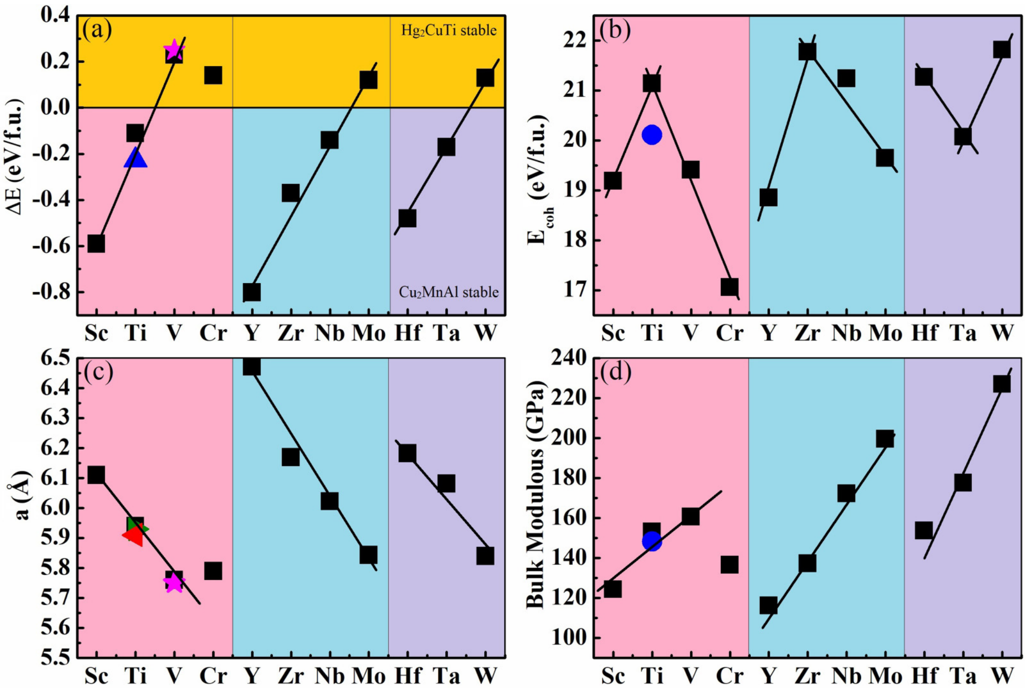

FIG. 2. Ground state structure parameters of Ni_2MnT (T = Sc, Ti, V, Cr, Y, Zr, Nb, Mo, Hf, Ta, and W) at theoretical equilibrium states: (a) The energy difference ΔE (in eV/f.u.) between the Cu_2MnAl-type (i.e., $L2_1$-type) and Hg_2CuTi-type structures of Ni_2MnT. The line in figure is to guide the eye to separate the Hg_2CuTi- or Cu_2MnAl-type structure, which corresponds to the positive and negative ΔE range, respectively. The other theoretical ΔE values of Ni_2MnTi (triangle) from Ref. [79] and Ni_2MnV (star) from Ref. [80] also are listed. (b) Cohesive energies E_{coh} (in eV/f.u.) of Ni_2MnT. The other theoretical E_{coh} (circle) for Ni_2MnTi is from Ref. [81]. (c) Lattice parameter a (in Å) of Ni_2MnT. The experimental and/or other theoretical lattice sizes of Ni_2MnT are from Refs. [15,81] (Ni_2MnTi, triangle) and [80,82] (Ni_2MnV, star). (d) Bulk modulus B (in GPa) of Ni_2MnT. The other theoretical bulk modulus (circle) of Ni_2MnTi is from Ref. [81]. Herein, the calculations in Refs. [80,82] and [79,81] were done by CASTEP and VASP, respectively.

structures. Notably, the crystal structures closely depend on preparation methods and subsequent heat-treatment technology; the further detailed experiments are encouraged to identify the feasible structures for currently studied Ni_2MnT compounds.

Under the abovementioned atomic preferential configuration, the lattice parameters of Ni_2MnT (T = Sc, Ti, V, Cr, Y, Zr, Nb, Mo, Hf, Ta, and W) were obtained by geometry optimization, as shown in Fig. 2(c). For T atoms in the same period, the lattice parameters of Ni_2MnT decrease with the increase in the number of valence electrons. Comparison of lattice parameters indicates that, for Ni_2MnT compounds, the bulk modulus follows the general trend that a larger bulk modulus corresponds to a smaller lattice size. Thus, the bulk modulus dependent on specific atoms shows inverse change behavior to the lattice size, as shown in Fig. 2(d). Currently, the difference in the lattice size among all-d-metal Heusler compounds originates from the atomic radii of transition metals. For atoms in the same period, their atomic radii decrease with the increase of valence electrons from left to right in the periodic table. The variation mode of the lattice parameter is dependent on specific atoms in Ni_2MnT compounds, which is like the distribution of the atomic size, as shown in Fig. 2(c). It indicates that the inherent atomic size is the main contributor of lattice parameters in all-d-metal Heusler compounds. However, in conventional Heusler compounds, the p-d covalent hybridization between 1nn main group elements and transition metals is also crucially important in determining the lattice size. In the main group element-rich compounds such as cubic $Mn_{2-x}CoGa_{1+x}$ [87] and tetragonal $Ni_{50}Mn_{5+x}Ga_{35-x}Cu_{10}$ [88] systems, the enhanced covalent hybridization results in kink behavior in the lattice parameter dependence of the main group element composition curve. Basically, in conventional Heusler compounds, the inherent atomic radius and the p-d hybridization codetermine the lattice size. Herein, in all-d-metal Heusler compounds, the main group elements are fully replaced with transition metals. As a result, covalent hybridization gets weakened, and it does not dominate the lattice size anymore. Experimentally, this weakened hybridization also lowered the atomic order level from prefect $L2_1$-type/Hg_2CuTi-type structure to partially disordered B2 structure or the mixture of $L2_1$-type/Hg_2CuTi-type and B2 structures [15]. For simplification, in current research, only fully ordered structures are considered. Theoretically, the calculated lattice constant of Ni_2MnTi was found to be 5.94 Å, which is very close to the experimentally observed value of 5.93 Å [15]. The marginal difference may originate from the disordered arrangement of atoms, which was experimentally observed in Ni_2MnTi. Furthermore, the theoretical lattice size of Ni_2MnV (5.76 Å) based on the EMTO method is consistent with the published values (5.75 Å) obtained by using the CASTEP code [80,82]. These agreements suggest that current calculations are practical. Based on these reliable calculations, the elastic properties, lattice dynamics, electronic structure,

TABLE I. Calculated elastic constants C_{ij} (in GPa), shear modulus G (in GPa), and melting temperature T_m (in K) for all-d-metal Heusler compounds Ni_2MnT (T = Sc, Ti, V, Cr, Y, Zr, Nb, Mo, Hf, Ta, and W). For comparison, the related parameters of well-known conventional Ni_2MnGa are also included here. Comparison done with experiments or previous calculations, wherever data are available as given.

	C_{11}	C_{12}	C_{44}	G_V	G_R	G_H	T_m
Ni_2MnSc	145.12	113.86	68.77	47.51	29.14	38.33	1410.81 ± 300
Ni_2MnTi	167.41	146.14	82.71	53.88	22.29	38.08	1542.59 ± 300
	157.3[a]	143.6[a]	73.7[a]				
Ni_2MnV	166.52	157.74	126.71	77.78	10.43	44.10	1537.28 ± 300
Ni_2MnCr	128.59	140.45	120.58	69.98	−16.01	26.99	1313.10 ± 300
Ni_2MnY	142.49	103.01	25.31	23.08	22.74	22.91	1395.25 ± 300
Ni_2MnZr	156.70	127.56	55.19	38.94	26.09	32.52	1479.24 ± 300
Ni_2MnNb	189.78	163.52	75.70	50.67	26.05	38.36	1674.81 ± 300
Ni_2MnMo	190.21	204.17	138.59	80.36	−18.89	30.74	1677.31 ± 300
Ni_2MnHf	180.20	140.53	58.67	43.14	32.90	38.02	1618.16 ± 300
Ni_2MnTa	185.37	173.78	68.10	43.18	12.85	28.01	1648.71 ± 300
Ni_2MnW	216.68	232.20	155.66	90.29	−20.96	34.67	1833.80 ± 300
	160.20	155.48	109.80	66.82	5.71	36.27	1499.78 ± 300
	163.6[a]	155.4[a]	106.7[a]				
	152[b]	143[b]	103[b]				
Ni_2MnGa	162.2[c]	157.07[c]	108.72[c]				
	166.7[d]	151.7[d]	113.4[d]				
	165.4[e]	149.4[e]	127.0[e]				

[a]Reference [81] by VASP.
[b]Reference [89] by experiments.
[c]Reference [90] by CASTEP.
[d]Reference [91] by EMTO.
[e]Reference [92] by EMTO.

and magnetism were investigated, and the discussion is presented in the following sections.

B. Elastic parameters determined martensitic phase transition and ductile properties

Based on the atomic configuration at the equilibrium states, elastic parameters of all-d-metal Heusler compounds Ni_2MnT (T = Sc, Ti, V, Cr, Y, Zr, Nb, Mo, Hf, Ta, and W) were calculated and listed in Table I. For comparative analysis, elastic parameters of well-studied Ni_2MnGa are also included herein. Table I presents the high consistency between our data about Ni_2MnGa and previous results, which again indicates that current calculations are valid and suitable to deal with Ni-Mn-based Heusler compounds.

All-d-metal Heusler compounds Ni_2MnT (T = Sc, Ti, V, Cr, Y, Zr, Nb, Mo, Hf, Ta, and W) exhibit cubic structures. They have three independent elastic constants, i.e., C_{11}, C_{12}, and C_{44}. Their sufficient and necessary mechanical stability conditions are given by (1) $C_{11} > 0$, (2) $C_{44} > 0$, (3) $C_{11} + 2C_{12} > 0$, and (4) $C' = \frac{C_{11}-C_{12}}{2} > 0$ [93]. The elastic constants summarized in Table I indicate that all the compounds satisfy the first three conditions well. The last condition of the tetragonal shear elastic constant C' is usually used to characterize the martensitic phase transition temperature (T_M), as shown in the equation of $\frac{dT_M}{dC'} = -\frac{1}{\beta C'}$, where $\beta = \frac{dC'}{TdT}$ [94]. Owing to softening, the β factor is always positive, so that the right side of the abovementioned equation is negative. Therefore, higher C' corresponds to lower T_M. This equation has been successfully adopted to discuss the possibility and tendency of martensitic phase transition in Ni-Mn-based Heusler compounds [95,96]. Furthermore, a perfect cubic Heusler compound is isotropic. The two shear moduli C' and C_{44} are equal, and the value of the Zener anisotropy factor (A) ($=\frac{2C_{44}}{C_{11}-C_{12}} = \frac{C_{44}}{C'}$) is 1. Commonly, A is considered a parameter to characterize the elastic anisotropy strength of cubic compounds. However, herein, it is used in a generalized manner to characterize the phase stability. Theoretically, any deviation of A from 1 indicates the instability of the cubic compounds. When the value of A is >2, the cubic compounds get transformed to low-symmetry martensitic phase [97,98].

In this paper, the tetragonal shear elastic constant C' and the Zener anisotropy factor (A) of Ni_2MnT (T = Sc, Ti, V, Cr, Y, Zr, Nb, Mo, Hf, Ta, W, and Ga) compounds at theoretical equilibrium states were calculated, and the corresponding results are shown in Fig. 3. Their validity as predictors of the phase stability has been verified, and they are still widely adopted in Ni-Mn-based Heusler compounds [100,101]. Obviously, compounds with late transition metals (T = Cr, Mo, and W) show negative C' and A, which indicates that martensitic phase transition can occur in them. Even though the values of C' and A in Ni_2MnV are both positive, they are comparable with the theoretical values of well-known Ni_2MnGa (see Fig. 3), which are very consistent with the published experimental data and theoretical results [89,90,92,100,102]. Thus, martensitic phase transition can also be expected in Ni_2MnV. In contrast, for compounds with early transition metals (T = Sc, Y, Zr, Nb, and Hf), their higher C' and lower A support more stable cubic structures. For Ni_2MnTi and Ni_2MnTa compounds, their medium values of C' and A indicate that the two compounds remain on the edge of the martensitic phase transition. Under certain external stimuli

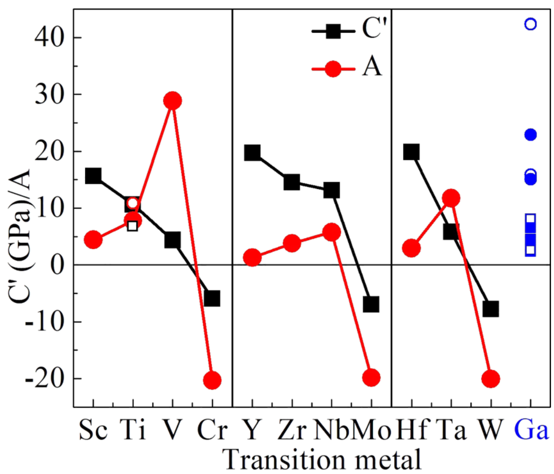

FIG. 3. Tetragonal shear elastic constant $C^{'}$ (in GPa) and Zener anisotropy factor (A) of Ni_2MnT (T = Sc, Ti, V, Cr, Y, Zr, Nb, Mo, Hf, Ta, and W) compounds at theoretical equilibrium states. These two parameters describe the possibility of martensitic phase transition. Other theoretical $C^{'}$ and A of Ni_2MnTi are from Ref. [81] by VASP. For comparative analysis, $C^{'}$ and A (in both, open blue circles are for theory, solid ones are for experiments) of Ni_2MnGa are also collected and included herein. These values are from this paper and Refs. [89,90,92,99]. Theoretical values in Refs. [90,92] and [92] were obtained by CASTEP and EMTO methods, respectively. The data in Refs. [89,99] are from experiments.

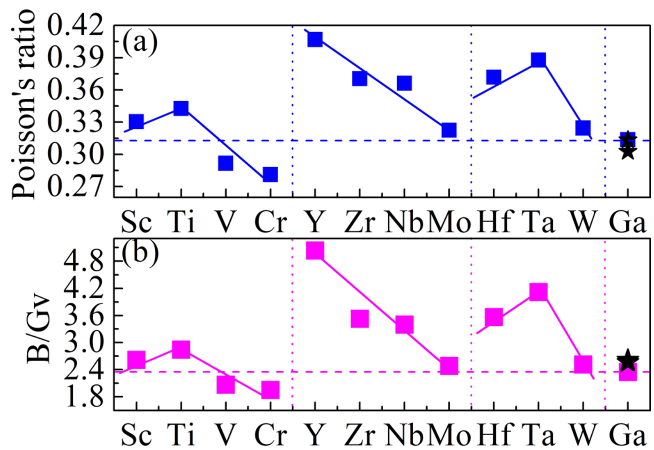

FIG. 4. Parameters describing the ductility of Ni_2MnT (T = Sc, Ti, V, Cr, Y, Zr, Nb, Mo, Hf, Ta, and W) compounds. (a) Poisson's ratio, (b) B/G_V ratio. For comparative analysis, parameters of well-known Ni_2MnGa are also included. The other Poisson's ratio and B/G_V ratio of Ni_2MnGa are obtained from Refs. [90,110] and [90,111], respectively. Herein, Ni_2MnT compounds with early transition metals show better ductility than conventional Ni_2MnGa and Ni_2MnT compounds with late transition metals. Therotical values in Refs. [90,111] were obtained by CASTEP and VASP methods, respectively. The data in Ref. [110] are from experiment.

such as high pressure and magnetic field, martensitic phase transition can be induced.

For conventional Heusler compounds, the directional covalent bonding between main group elements and transition metal atoms leads to inherent brittleness, seriously affecting their service performance. To improve the ductile properties and satisfy more flexible applications, one ideal and effective way is to design Heusler compounds with less covalent bonding. Thus, all-d-metal Heusler compounds have attracted more attention and have become popular. Other than the outstanding functional properties, great improvements in ductility can also be expected. For all-d-metal Heusler compounds Ni_2MnT (T = Sc, Ti, V, Cr, Y, Zr, Nb, Mo, Hf, Ta, and W), the ductile properties are evaluated from Poisson's ratio (υ) and the B/G ratio, followed by the discussion on interatomic orbital hybridization style from calculated ELF. Herein, these adopted methods and theories are still widely used to reasonably evaluate the ductility and reveal its physical origin in materials, including but not limited to cubic Heusler compounds [18,103–106].

By using the Voigt-Reuss-Hill (VRH) approximation, elastic moduli were obtained herein from the elastic constants of a single crystal [107–109]. With the help of Voigt and Reuss approximations, the bulk and shear moduli of cubic Heusler compounds were derived by $B_V = B_R = \frac{C_{11}+2C_{12}}{3}$, $G_V = \frac{(C_{11}-C_{12}+3C_{44})}{5}$, and $G_R = \frac{5(C_{11}-C_{12})C_{44}}{4C_{44}+3(C_{11}-C_{12})}$. Based on VRH approximation, average bulk and shear moduli ($B_H = \frac{B_V+B_R}{2}$ and $G_H = \frac{G_V+G_R}{2}$) can be deduced. The detailed shear moduli are listed in Table I. Furthermore, by $\nu = \frac{3B-2G}{2(3B+G)}$, Poisson's ratio (details in Fig. 4) was obtained. First, the ductility of Ni_2MnT compounds was directly evaluated from Poisson's ratio. In general, materials with $\upsilon > \frac{1}{3}$ are ductile, whereas those with $\upsilon < \frac{1}{3}$ are brittle. Figure 4(a) illustrates that the calculated υ of well-studied Ni_2MnGa (=0.31) is less than the empirical boundary value, indicating its brittle nature. This claim agrees with previous observations [14,112] and further proves the validity of the current calculations. In contrast, all-d-metal Heusler compounds Ni_2MnT (T = Sc, Ti, V, Cr, Y, Zr, Nb, Mo, Hf, Ta, and W) show different ductility. Compounds with early transition metals, i.e., Sc, Ti, Y, Zr, Nb, Hf, and Ta, possess higher υ values, which are all above critical value and consequently exhibit better ductility. Instead, compounds with late transition metals, i.e., V, Cr, Mo, and W, show lower υ values, which are below the separating line and drive these compounds to be brittle. Second, based on Pugh's research, the B/G ratio was proposed as another parameter to separate brittle and ductile materials [113]. The boundary value to separate ductile and brittle materials is ~1.75. Commonly for materials, the higher the B/G ratio, the more the ductile nature and vice versa [113]. A previous related study about Ni-Mn-based Heusler compounds indicates that the B/G_V ratio based on G_V can serve as a better parameter to separate ductile and brittle systems [90,103]. For Ni_2MnT (T = Sc, Ti, V, Cr, Y, Zr, Nb, Mo, Hf, Ta, and W) compounds investigated herein, all B/G_V ratios are above the critical value. Thus, these all-d-metal Heusler compounds can be considered ductile materials from the perspective of the B/G_V ratio. This is different from the judgment by Poisson's ratio. Owing to the fact that the critical value of Poisson's ratio used herein was not defined explicitly in the literature and only based on properties reported for the materials tabulated by Frantsevich [114], it is an empirical separating line practically. Finally, although the classification is imprecise, both the B/G_V ratio and Poisson's ratio of compounds with early

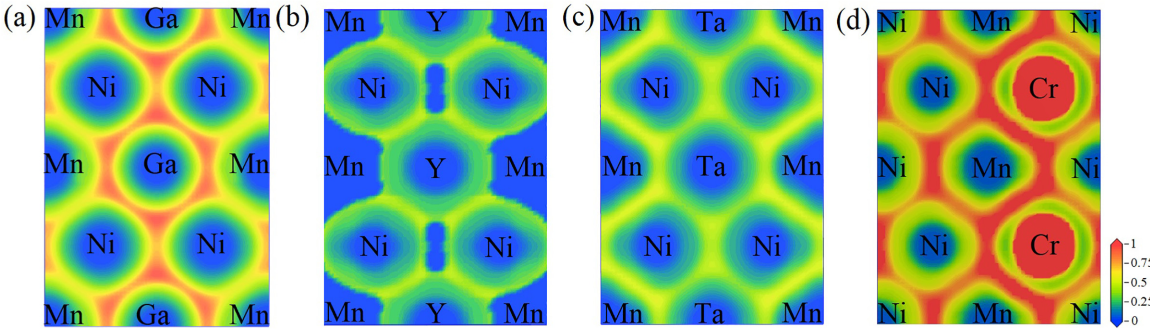

FIG. 5. Electron localization function (ELF) distributions of (a) Ni_2MnGa, (b) isostructural Ni_2MnY, and (c) Ni_2MnTa in Cu_2MnAl-type structure, and (d) Ni_2MnCr in Hg_2CuTi-type structure on (110) plane of unit cell. The scale bar from blue to red corresponds to increasing electron localization (namely, increasing covalent bonding). Compared with Ni-Y and Ni-Ta atom pairs in Ni_2MnY and Ni_2MnTa, there are higher values between Ni-Ga atom pairs in Ni_2MnGa.

transition metals are higher than those of conventional Ni_2MnGa and Ni_2MnT compounds consisting of late transition metals V, Cr, Mo, and W. This is clearly illustrated in Figs. 4(a) and 4(b).

Inherently, ductile performance in solids can be directly reflected from the angular character of bonding between constituent atoms. Physically, covalent bonding is directional with the angular character and responsible for brittleness and lower ductility in solids [115]. To discuss trends in chemical bonding and reveal the mechanism of enhanced ductility in Ni_2MnT compounds with early transition metals compared with Ni_2MnGa, representative ELFs [116,117] of Ni_2MnGa, Ni_2MnY, Ni_2MnTa, and Ni_2MnCr were calculated and shown in Fig. 5. The ELF is often used to investigate the nature of chemical bonding in different types of materials [88,118]. For instance, in Cu_2MnAl-type Ni_2MnGa, Ni_2MnY, and Ni_2MnTa, the Ga, Y, and Ta atoms locate in the cubic crystal field with 8 Ni atoms as their 1nn atoms. It provides a convenient platform to investigate the change of chemical bonding by comparing Ni-Ga, Ni-Y, and Ni-Ta bonding. The topological analysis of the ELF indicates the occurrence of strong covalent hybridization between Ga and Ni atoms in Ni_2MnGa, which results from the *p-d* orbital hybridization between *p* electrons of Ga and *d* electrons of Ni atoms. It shows an obvious directional character. The brittleness in the intermetallic compound Ni_2MnGa could intrinsically originate from this interatomic covalent hybridization. However, in all-*d*-metal Heusler compounds Ni_2MnY and Ni_2MnTa, the interatomic covalent hybridization strength between Y/Ta and Ni atoms decreases significantly. Correspondingly, the metallic bonding becomes dominant and does not remain directional anymore. Thus, the increased metallic bonding could be largely responsible for the enhancement of ductility in Ni_2MnY and Ni_2MnTa. Similar comparisons of ELFs between Ni_2MnGa and Ni_2MnTi compounds were also investigated, as presented in Fig. S4 in the Supplemental Material [25] and Refs. [61,81]. However, in Hg_2CuTi-type Ni_2MnCr, it is another case. The interatomic covalent hybridization in Hg_2CuTi-type Ni_2MnCr is obviously stronger compared with Ni_2MnGa, which results in lower ductile parameters, as presented in Fig. 4.

Practically and importantly, due to the relatively low energy of metallic bonding compared with covalent bonding, the nucleation and propagation of dislocation in real metallic bonding materials become relatively easy since the energy consumed to overcome bond distortion and breaking decreases [30]. It is speculated that this may result in higher density of dislocation and corresponding increase in plastic performance of all-*d*-metal Heusler compounds Ni_2MnT ($T =$ Sc, Ti, Y, Zr, Nb, Hf, and Ta). Combining the calculated ELFs, significant enhancement in ductile properties was experimentally observed in Ni-Mn-Ti compounds [18,60,61], which can be mainly ascribed to improved metallic bonding. Thus, based on chemical bonding engineering, tuning the bonding type of interatomic coupling has been proven to be an effective approach to design high-ductility multiple functional materials.

For engineering applications, the thermodynamic properties are also significantly important. Herein, this issue is discussed from the perspective of the melting point. Empirically, it can be obtained by using an approximate equation of $T_m = 553\ \mathrm{K} + \frac{5.91\mathrm{K}}{\mathrm{GPa}} C_{11}$, in which C_{11} is elastic constant, as presented in Table I. The standard error is about ± 300 K [119]. Notably, good agreements with experiments were achieved by this method to predict melting points in cubic compounds [120]. Herein, the calculated melting point for Ni_2MnGa is 1499.78 ± 300 K. Its experimental value is 1380 K [121], which lies well in the confidence interval of the calculated value. Again, this agreement confirms the feasibility of our calculation. Based on this method, melting points of Ni_2MnT ($T =$ Sc, Ti, V, Cr, Y, Zr, Nb, Mo, Hf, Ta, and W) compounds were obtained and are listed in Table I. In general, a higher melting point indicates a stronger resistance to temperature. Thus, the high melting point values of Ni_2MnT ($T =$ Sc, Ti, V, Cr, Y, Zr, Nb, Mo, Hf, Ta, and W) compounds indicate that their ground state properties can be preserved as much as possible when temperature is increased [115,122]. It enables these compounds to serve more flexible situations. The melting points of Ni_2MnT predicted in this paper call for further experimental study for verification. Furthermore, systematic investigations are required to increase the accuracy of the method to predict the melting point of Heusler compounds.

For a reliable evaluation of the martensitic phase transition in cubic compounds, electronic structure and phonon dispersion were also involved and are discussed in the following

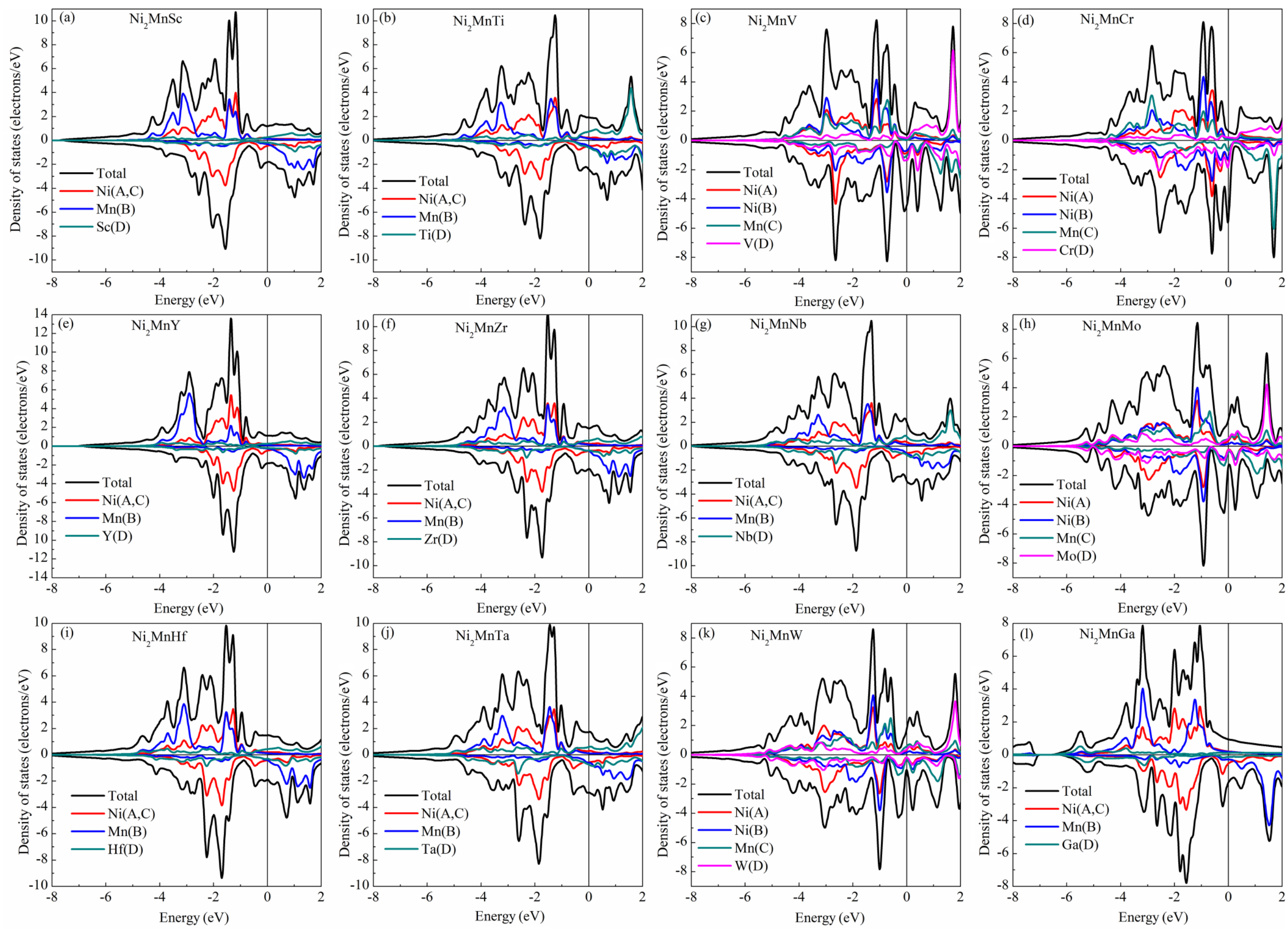

FIG. 6. (a)–(k) Calculated spin-projected density of states (DOS) plots of Ni_2MnT (T = Sc, Ti, V, Cr, Y, Zr, Nb, Mo, Hf, Ta, and W) compounds. The total and partial DOSs for d electrons of atoms on specific crystalline sites are included. The upper halves of each panel display the spin-up states. For comparison, the DOSs of Ni_2MnGa are illustrated in (l). Herein, the DOSs of Ni_2MnGa, Ni_2MnV, and Ni_2MnTi are like those by CASTEP (for Ni_2MnGa in Ref. [90] and Ni_2MnV in Ref. [82]) and VASP (for Ni_2MnTi in Ref. [81]).

sections. Importantly, comprehensive analysis of these factors can aid in achieving consistent conclusions about the martensitic phase transition of cubic Ni_2MnT compounds.

C. Electronic structures

The electronic structure information at the ground state, such as DOS, depends on the specific crystal structure and directly reflects physical properties of materials. In conventional Ni_2Mn-based Heusler compounds, the structural instability of the cubic phase was characterized by the typical peak structure below the Fermi level (E_F) in the spin-down band. This peak structure predominantly stemmed from Ni 3d eg orbitals (for details, see Refs. [123–126]). In conventional Ni_2Mn-based Heusler compounds, it can result in the band Jahn-Teller instability of the cubic structures [126–128]. Thus, this peak structure can usually serve as an intuitive criterion in determining the phase stability of Heusler compounds. To further clarify the physical origin of the stability in cubic Ni_2MnT compounds, the spin-polarized total and partial DOSs were calculated herein, and the corresponding results are shown in Fig. 6 for analysis. Herein, the DOSs of all compounds show peak structures just below E_F in the spin-down band (0 to −0.6 eV). Dependent on specific transition metals, the DOSs of Ni_2MnT (T = Sc, Ti, V, Cr, Y, Zr, Nb, Mo, Hf, Ta, and W) compounds near E_F manifest diverse distributions. Among all compounds studied herein, Ni_2MnV, Ni_2MnCr, Ni_2MnMo, and Ni_2MnW show typical peak structures below E_F, as observed in well-known Ni_2MnGa. Moreover, these peaks possess relatively high values compared with the remaining Ni_2MnT compounds investigated in this paper. Different from the case of Ni_2MnGa, the 3d states of Ni and T (=V, Cr, Mo, and W) atoms all contribute to these prominent peak structures below E_F. These prominent peak structures near E_F, more often than not, cause high energy and consequently lead to poor structural stability in the parent cubic phase [81,127,129]. A tetragonal distortion is an effective way to reduce the peak structures near E_F and avoid the instability [130]. Thus, the most likely tetragonal distortion can be expected in Ni_2MnV, Ni_2MnCr, Ni_2MnMo, and Ni_2MnW. In high-symmetry Heusler compounds, the equivalent k points in the Brillouin zone lead to the same band energies. Owing to tetragonal distortion, some originally equivalent k points become inequivalent, leading to unequal energy values at

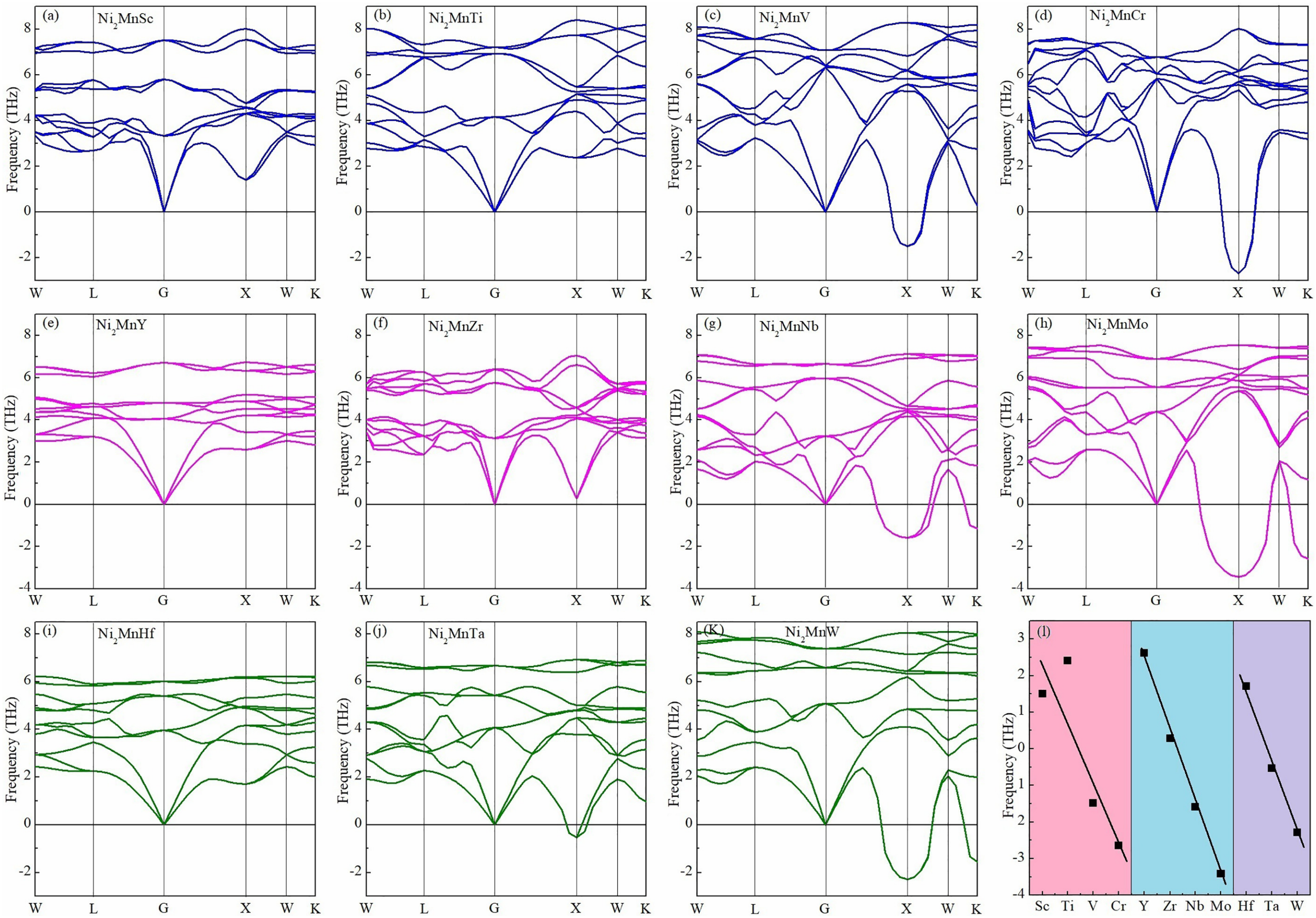

FIG. 7. (a)–(k) The calculated phonon dispersions of Ni_2MnT (T = Sc, Ti, V, Cr, Y, Zr, Nb, Mo, Hf, Ta, and W) compounds. Imaginary frequencies of the unstable modes are shown in negative frequency range. The high-symmetry q point path in the Brillouin zone is chosen as $W(0.5,\ 0.25,\ 0.75) \rightarrow L(0.5,\ 0.5,\ 0.5) \rightarrow G(0,\ 0,\ 0) \rightarrow X(0.5,\ 0,\ 0.5) \rightarrow W(0.5,\ 0.25,\ 0.75) \rightarrow K(0.375,\ 0.375,\ 0.75)$. Frequency values at the X point dependent on specific transition metal atoms are presented in (l).

these points and consequently smooth distribution of DOSs near E_F [129]. Moreover, due to tetragonal distortion, the symmetry of the system gets lowered. The degenerate bands in the cubic system do not remain degenerate in the tetragonal system. Bands that overlap in the direction of contraction become broader. A repopulation of electrons was allowed to avoid the electronic instability of the band Jahn-Teller type [131,132]. All these effects can smoothen the peak structures of DOSs near E_F and lower the energy of the cubic phase.

Owing to similar electronic configurations of Sc, Ti, Y, Zr, Nb, Hf, and Ta, the DOSs of Ni_2MnT (T = Sc, Ti, Y, Zr, Nb, Hf, and Ta) compounds distribute in a similar manner in the entire energy span. Their peak structures below E_F are shallow with relatively low values. Thus, comparison with Ni_2MnV, Ni_2MnCr, Ni_2MnMo, and Ni_2MnW indicates that their peak structure characteristics are weaker. The cubic structures in these compounds are relatively stable. All judgments about the phase stability of Ni_2MnT (T = Sc, Ti, V, Cr, Y, Zr, Nb, Mo, Hf, Ta, and W) compounds are consistent with the evaluation based on the elastic moduli, strongly supporting the current assessment.

D. Lattice dynamics properties

For an in-depth investigation of the dynamic stability of Ni_2MnT (T = Sc, Ti, V, Cr, Y, Zr, Nb, Mo, Hf, Ta, and W) compounds, the phonon dispersions along the symmetry line at ground state were calculated, and the corresponding results are shown in Fig. 7. In phonon dispersion curves of Ni_2MnT (T = Sc, Ti, V, Cr, Y, Zr, Nb, Mo, Hf, Ta, and W) compounds, the most important phenomenon is the softening of two transverse acoustic (TA) phonon modes along G-X-W directions, all reaching a local minimum at the X point of the Brillouin zone. Figure 7(l) demonstrates that these minima dependent on specific transition metal atoms gradually become weak with the increase of valence electrons in each period of periodic table. The minima of Ni_2MnT with late transition metal atoms locate at obvious imaginary frequencies zone. Compared with experimental phonon dispersions in Ni-Mn-Ga compounds [133,134], these anomalies strongly indicate that cubic phases of Ni_2MnT with late transition metal atoms are unstable to shear deformation corresponding to the eigenvector of TA modes. Possible martensitic phase transition can be expected in them. Thus, these abnormal softening behaviors of TA modes closely relate to

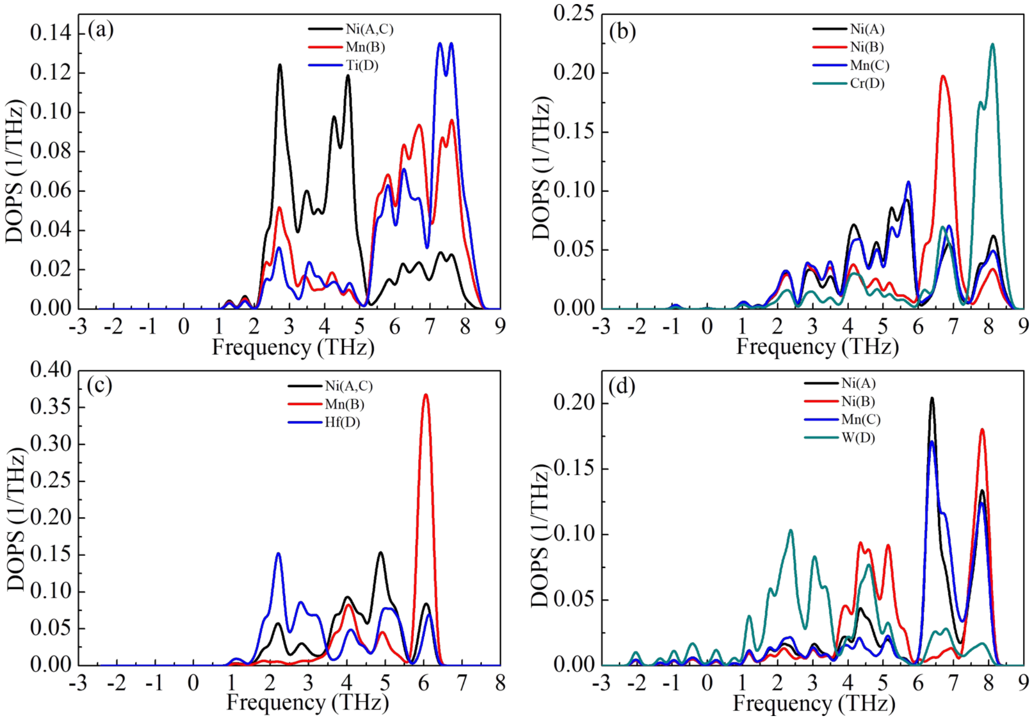

FIG. 8. (a)–(d) The selected site projected phonon density of states of Ni_2MnTi, Ni_2MnCr, Ni_2MnHf, and Ni_2MnW, respectively, showing the distribution of amplitudes of atoms in the frequency range. In Ni_2MnCr and Ni_2MnW, the visible anomalous behavior of medium frequencies phonon dispersions of Mn(C), which lie below the optical modes of those heavier Ni(B) atoms, is to act via hybridization as a repulsive force on the transverse acoustic modes.

C'. The lower the value of C', the more unstable the cubic phase [115]. The relative phase stability of Ni_2MnT (T = Sc, Ti, V, Cr, Y, Zr, Nb, Mo, Hf, Ta, and W) compounds is consistent with the judgment made based on elastic parameters.

To further identify the origin of these anomalous softening behaviors, the partial phonon DOSs of Ni_2MnTi, Ni_2MnCr, Ni_2MnHf, and Ni_2MnW were analyzed and are presented in Fig. 8. The sequence of atomic contribution to phonon dispersions is mainly separated by mass. Normally, heavier atoms dominate the low-frequency phonon modes and vice versa [128,135]. In Ni_2MnTi and Ni_2MnHf, the atomic contribution to phonon dispersions shows the normal sequence, resulting in stable states without obvious softening. However, in both Ni_2MnCr and Ni_2MnW, Mn(C) atoms dominate the medium frequency phonon dispersions, which lie below the optical modes of heavier Ni(B) atoms. This inversion acts via hybridization as a repulsive force on the acoustic modes and leads to the deep softening of low-lying TA phonon modes [128]. Moreover, consistent judgments on the stability of Ni_2MnTi, Ni_2MnCr, Ni_2MnHf, and Ni_2MnW from the perspective of both phonon dispersions and DOSs indicate the occurrence of strong interaction between electronic structure and phonon dispersion [136,137]. Undeniably, a lot more systematic explorations and experiments, such as inelastic neutron scattering, are further demanded to verify the phonon dispersions and to make comparison with available results of conventional Ni-Mn-based shape memory Heusler compounds.

E. Pressure-induced martensitic phase transition in Ni_2MnTi

According to the literature, pressure can reduce magnetism and volume, which provides an effective and clear approach to tune the phase stability of cubic Ni-Mn-based Heusler compounds [2,3,5,8]. Herein, considering the Ni_2MnTi compound as a representative example, the effect of external pressure on the cubic phase stability of strongly ferromagnetic all-d-metal Heusler compounds was investigated, as shown in Fig. 9. First, Fig. 9(a) exhibits that the application of pressure suppresses the spin polarization of Ni_2MnTi and decreases its magnetic moment. Herein, the calculated magnetic moment of Ni_2MnTi at ground state is 4.33 μ_B/f.u., which can be comparable with published values (4.07 μ_B/f.u. in Ref. [81] and 3.90 μ_B/f.u. in Ref. [79]) by VASP. The loss of the magnetic moment is also accompanied by shrinkage of the lattice size when pressure is applied. Thus, it is speculated that loss of magnetism and contracted lattice size can destabilize the cubic phase [138]. Second, due to bond stretching in the shrunken cubic structure [139], TA modes in phonon dispersions gradually shift to the lower frequency zone with the increase of pressure, as shown in Fig. 9(b). TA branching along G-X-W directions shows the obvious softening as a function of pressure. As expected, when pressure is 16 GPa and beyond in Fig. 9(c), low-lying TA branches along G-X-W directions anomalously move to negative frequency ranges. This softening character of TA branches indicates that the cubic structure becomes dynamically unstable and martensitic phase transition can occur when the pressure is applied. Third, the pressure-induced martensitic phase transition in Ni_2MnTi can

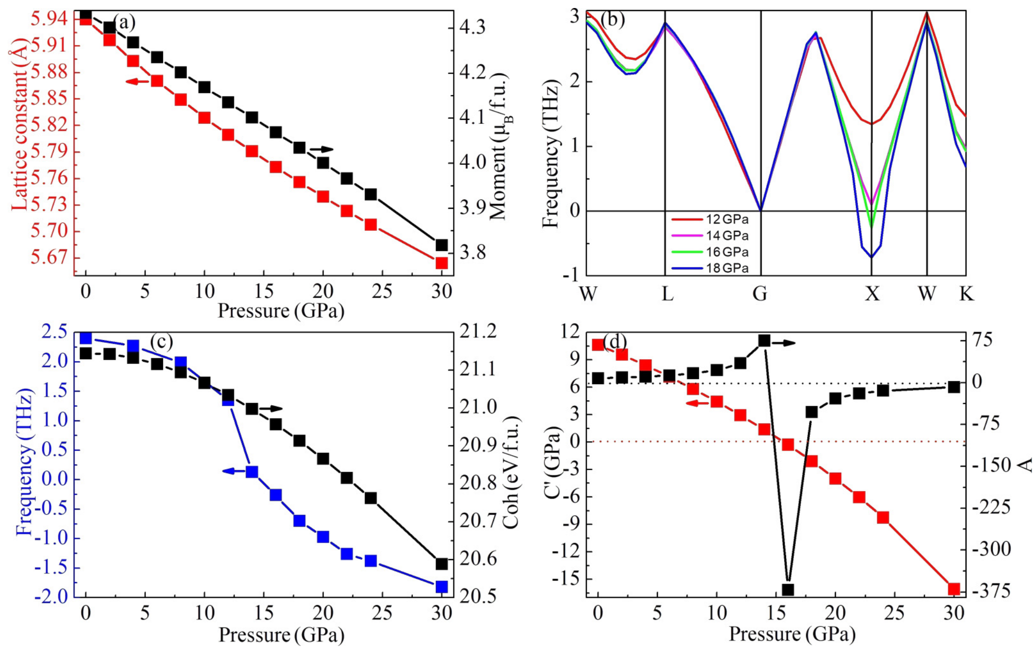

FIG. 9. Pressure dependence of physical parameters, indicating martensitic phase transition in Ni_2MnTi: (a) Pressure dependence of lattice parameter and magnetic moment. (b) Phonon dispersions of low-lying transverse acoustic (TA) branches at 12, 14, 16, and 18 GPa. The occurrence of imaginary frequency at 16 GPa indicates that applied pressure destabilizes cubic structure. (c) TA frequencies at high-symmetry point X and cohesive energy as a function of pressure. (d) Pressure dependence of tetragonal shear elastic constant $C^{'}$ and Zener anisotropy factor (A). Their change behaviors support pressure-induced martensitic phase transition in Ni_2MnTi.

also be supported by the calculations of tetragonal shear elastic constant C' and Zener anisotropy factor (A). Figure 9(d) illustrates that the values of C' and A at the pressure of 14 GPa are ~1.38 GPa and 75.38, respectively. These values are close to theoretical values ($C' = 2.36$ GPa, $A = 42.43$ in this paper derived from data presented in Table I) and experimental results of well-studied Ni_2MnGa [89,90,92,99,100,102]. The values of C' and A both become negative when the pressure reaches 16 GPa and beyond. Furthermore, the decreased cohesive energy under pressure also destabilizes cubic Ni_2MnTi.

Importantly, when external pressure is applied on Ni_2MnTi, the inherent nature of unit cell size contraction during martensitic phase transition shortens the interatomic distance and consequently leads to the enhancement in the d-d interatomic orbital hybridization [138]. The enhanced d-d interatomic orbital hybridization can result in the improvement of ductility in Ni_2MnTi. Theoretically, ductile parameters of Poisson's ratios and B/G_V ratios shown in Fig. 10 both get improved when pressure is applied on Ni_2MnTi, indicating better ductile properties. Practically, the enhanced ductility can benefit the future application of the barocaloric and elastocaloric effects in all-d-metal Heusler compounds.

Owing to the difference between atomic radii in the all-d-metal Heusler compound Ni_2MnTi, the so-called *chemical pressure* can be induced during atomic substitution, which can work like the applied external hydrostatic pressure when tuning the phase stability. Herein, the phase stability of off-stoichiometric $Ni_2Mn_{1+x}Ti_{1-x}$ compounds was theoretically investigated. The dependence of calculated C' and experimental martensitic phase transition temperature (T_M) on Ti content is shown in Fig. 11. As indicted by the circle in Fig. 11, the linearly fitted T_M value of Ni_2MnTi is near zero. It indicates fewer possibilities of martensitic phase transition in stoichiometric Ni_2MnTi, which is consistent with the judgment from obtained elastic parameters, electronic structure, and phonon dispersion. Experimentally, martensitic phase transition was not observed in Ni_2MnTi even when temperature was decreased significantly to 50 K [15]. When Ti was doped with Mn in $Ni_2Mn_{1+x}Ti_{1-x}$ compounds, the C' could be softened and even made negative, as shown in Fig. 11, which led to the decreased stability of cubic structure and experimentally led

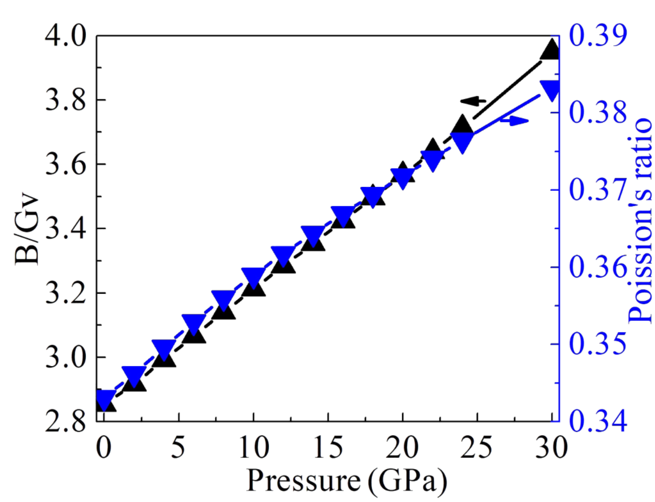

FIG. 10. Pressure dependence of ductile parameters of B/G_V ratio and Poisson's ratio in Ni_2MnTi. Their synchronous increase under applied pressure shows improved ductility.

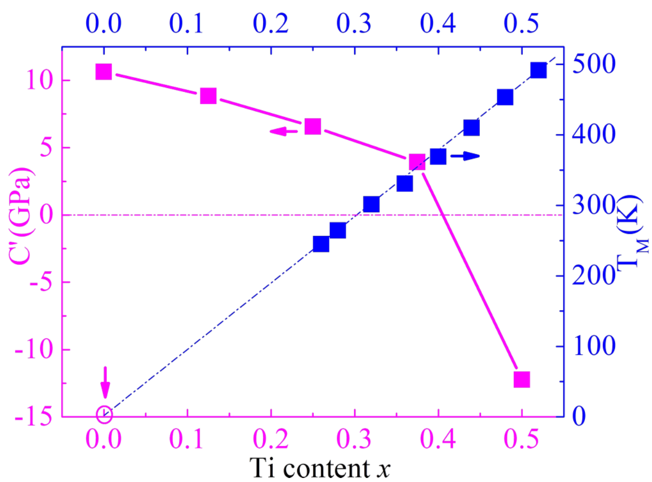

FIG. 11. Ti content x dependence of tetragonal shear elastic constant C' and experimental martensitic phase transition temperature (T_M) in $Ni_2Mn_{1+x}Ti_{1-x}$ ($x = 0$–0.5) Heusler compounds. T_M was selected from Refs. [15,18]. The circle and arrow indicate that the martensitic phase transition temperature of stoichiometric Ni_2MnTi is near zero.

to T_M of $Ni_2Mn_{1+x}Ti_{1-x}$ being up to room temperature when x was ~0.30 [15,18,19]. This changing behavior of dependence of phase transition temperature on composition is very similar to that observed in conventional $Ni_2Mn_{1+x}Z_{1-x}$ (Z = Al, Ga, In, Sn, Sb) compounds [16].

When the smaller Mn atom dopes larger Ti atoms, the lattice size of $Ni_2Mn_{1+x}Ti_{1-x}$ compounds decreases gradually with the increase of doping content of Mn [15]. Figures 9(a) and 9(d) present the lattice size and C' of stoichiometric Ni_2MnTi, revealing that C' decreases with the contraction of lattice size. From this perspective, the decrease of C' and consequently the instability of cubic $Ni_2Mn_{1+x}Ti_{1-x}$ compounds could result from the contribution of volume effect. Comparison of the lattice size dependence of C' in off-stoichiometric $Ni_2Mn_{1+x}Ti_{1-x}$ and stoichiometric Ni_2MnTi reveals that C' in off-stoichiometric $Ni_2Mn_{1+x}Ti_{1-x}$ decreases far faster than that in stoichiometric Ni_2MnTi (see Fig. S5 in the Supplemental Material [25]). This difference indicates that the change of instability in off-stoichiometric $Ni_2Mn_{1+x}Ti_{1-x}$ is not merely a volume effect. Moreover, in off-stoichiometric $Ni_2Mn_{1+x}Ti_{1-x}$, the valence electron concentration increases with the increase of Mn content since Mn possesses more valence electrons than Ti. In general, the larger the valence electron concentration, the higher the martensitic phase transition temperature. It suggests that the increased valence electron concentration lowers the stability of cubic structure, which corresponds to the smaller value of C'. Therefore, the faster decrease of C' in off-stoichiometric $Ni_2Mn_{1+x}Ti_{1-x}$ also results from the contribution of the increased valence electron concentration. Thus, in $Ni_2Mn_{1+x}Ti_{1-x}$ compounds, the coupling of the volume effect and valence electron concentration is responsible for the changes of phase stability and consequently martensitic phase transition temperature.

F. Atomic diffusion process arrest-induced antiferromagnetism in Ni_2MnTi

Mn-containing Heusler compounds have become popular subjects of investigation because of their interesting feature of forcing the Mn atoms to occupy the sites with different neighboring relationships. This allows them to exchange couple in a ferromagnetic, ferrimagnetic, antiferromagnetic order, and even nonmagnetic manner [87,88,115]. Like conventional Ni-Mn-based Heusler compounds, Ni_2MnTi was theoretically predicted to be stable in ferromagnetic $L2_1$-type structure at ground state [79,81]. Notably, the Mn atom is the key contributor of magnetism. Rather differently, experimental magnetization measurements revealed that the Ni_2MnTi compound was antiferromagnetic, characterized by a low Néel temperature. Disordered arrangement of Mn and Ti atoms in metastable B2 structure was considered responsible for antiferromagnetism [15]. It indicates that antiferromagnetism can result from the disordered arrangement of Mn and its neighboring atoms.

To better comprehend and explore the origin of antiferromagnetism in Ni_2MnTi, five possible interatomic occupation styles were considered assuming that Ni_2MnTi remained in Cu_2MnAl-type and Hg_2CuTi-type structures: (i) atomic disorder between Mn(B) and Ti(D), Ni(A, C) in Cu_2MnAl-type structure and (ii) atomic disorder between Mn(C) and Ni(A), Ni(B), and Ti(D) in Hg_2CuTi-type structure. The total magnetic moments of Ni_2MnTi dependent on interatomic disorder level under these five possible disorderly arranged styles are shown in Figs. 12(a) and 12(b). The quantity of interatomic disorder level S is defined as follows:

$$S = \frac{\text{No. of A atoms on sublattice A when fully ordered} - \text{No. of A atoms on sublattice A when disordered}}{\text{No. of A atoms on sublattice A when fully ordered}}.$$

Other than the experimentally obtained disordered arrangement style between B and D sites in Cu_2MnAl-type structure [15], theoretical interatomic disordered occupation between Ni(A, C) and Mn(B) in the Cu_2MnAl-type structure, and Mn(C) and Ni(B)/Ti(D) in the Hg_2CuTi-type structure can also induce antiferromagnetism in Ni_2MnTi. Compared with the high-ordered ferromagnetic ground state of the Ni_2MnTi compound, the antiferromagnetic state in disordered Ni_2MnTi was found to be metastable, which is like those theoretically observed in B2-type $Ni_8Mn_5Ti_3$ [61]. To further explore the most possible occupation style of atoms at finite temperature and their physical origin, the energy dependent on the disorder level at the PM state was calculated, and the results are presented in Figs. 12(c) and 12(d). At PM states, when disordered occupation occurs between Mn and Ti in Ni_2MnTi [i.e., Mn(B) and Ti(D) in the Cu_2MnAl-type structure, and Mn(C) and Ti(D) in the Hg_2CuTi-type structure], the total energy dependent on the disorder level increases at a certain disorder

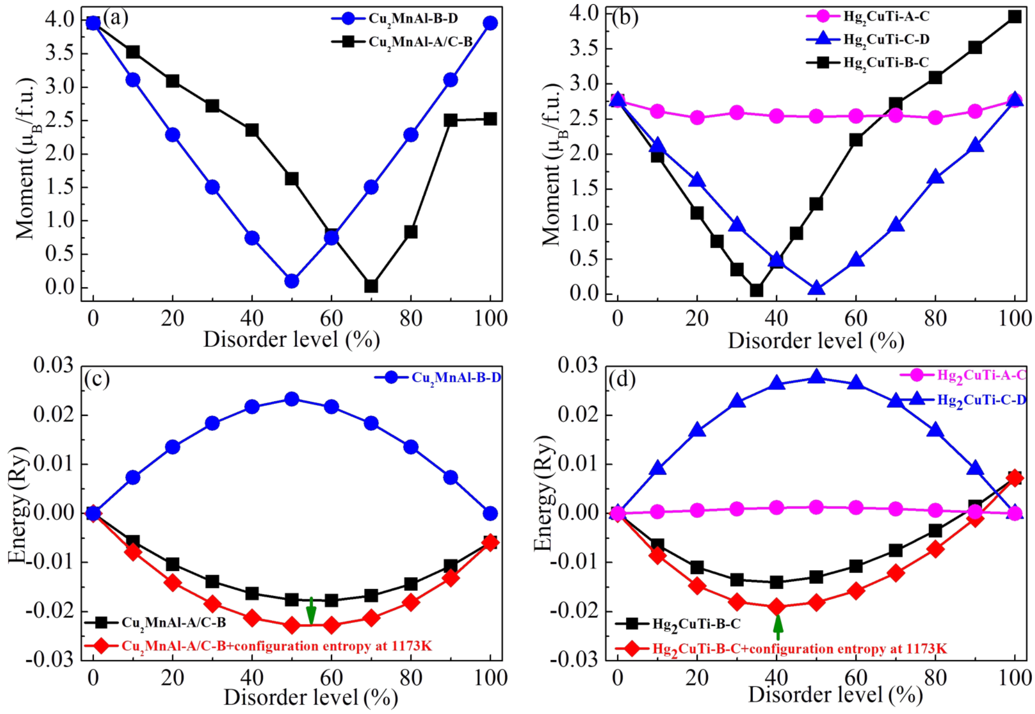

FIG. 12. Disorder-level dependence of magnetic moment in Ni_2MnTi at ground state with (a) Cu_2MnAl-type and (b) Hg_2CuTi-type structures. The local minimum indicates antiferromagnetism. Relative paramagnetic (PM) total energy and PM total energy plus the contribution from the configuration entropy at 1173 K as a function of the disorder level at PM state in Ni_2MnTi with (c) Cu_2MnAl-type and (d) Hg_2CuTi-type structures, considering the ground state energy of the ordered Ni_2MnTi as reference. The green arrows in (c) and (d) indicate the energy minimum at disorder level of ∼55 and 40% with Cu_2MnAl- and Hg_2CuTi-type structures, respectively.

range and reaches a local maximum at the disorder level of ∼50%. This is not a favorable condition at the PM state. Inversely, when atomic disorder occurs between Mn and its 1nn Ni in Ni_2MnTi [i.e., Mn(B) and Ni(A/C) in the Cu_2MnAl-type structure, and Mn(C) and Ni(B) in the Hg_2CuTi-type structure], the PM total energy dependence of the disorder level shows a local minimum at the disorder level of ∼56% in the Cu_2MnAl-type structure and ∼38% in the Hg_2CuTi-type structure. It indicates stable atomic configurations at PM states. Furthermore, by considering the configuration entropy at 1173 K (representing the experimental annealing temperature in Ref. [15]), the energy minima become significantly low [see Figs. 12(c) and 12(d)], indicating more stable states. Furthermore, at 1173 K, the preferential disorder levels are ∼55% in the Cu_2MnAl-type structure and ∼40% in the Hg_2CuTi-type structure, showing only slight changes with temperature. Comparatively, the dependence of the energy of a local minimum on disorder level curve of the Hg_2CuTi-type structure is lower than that of the Cu_2MnAl-type structure, which indicates that the Hg_2CuTi-type structure becomes dominant at the high-temperature PM state. It is expected that, when the atomic disordered arrangement occurs either between Mn(B) and Ni(A/C) in the Cu_2MnAl-type structure or between Mn(C) and Ni(B) in the Hg_2CuTi-type structure, Ni_2MnTi can remain in a mixture of Hg_2CuTi- and Cu_2MnAl-type structures. Consequently, current calculations and analysis reveal that the disordered occupation of atoms between Mn and its 1nn Ni atoms is preferential in Ni_2MnTi around the experimental annealing temperature, where it is in the PM state.

Based on the above-stated calculation results, the following scenario was suggested to reveal the physical origin of experimentally observed antiferromagnetism in Ni_2MnTi. When Ni_2MnTi was cooled down from the high-temperature PM state, the disorder-order transition during the cooling processes aided in determination of atomic configuration and consequently the magnetic states. Commonly, the complete atomic diffusion process during cooling can promise a full transformation from the high-temperature atomic disordered PM state to the chemically and magnetically ordered ferromagnetic state. Otherwise, any atomic diffusion process arrest can change the ultimate magnetic state. When quenching Ni_2MnTi from the PM state at 1173 K, the shortened atomic diffusion process blocks the transition from the atomic disordered PM state to the ordered ferromagnetic state. Owing to the atomic diffusion process arrest during cooling process, Ni_2MnTi gets locked in an intermediate state, which consequently maintains the relatively high atomic disorder level inherited from the high-temperature PM state. The atomic disorder level cannot further evolve toward the ordered ferromagnetic state anymore. Thus, the generation of the antiferromagnetic Ni_2MnTi is due to the incomplete transition from the high-temperature PM state to the ferromagnetic state when cooling. Further neutron diffraction experiments are encouraged to confirm the above-discussed atomic occupation styles. Our current theoretical observations indicate that suitable thermodynamics states when annealing and the atomic diffusion process when cooling the samples are crucial for optimizing magnetic states and further realizing their functional applications.

IV. CONCLUSIONS

In this paper, the elastic properties, phase stability, and magnetism and correlations among them in all-d-metal Ni_2MnT (T = Sc, Ti, V, Cr, Y, Zr, Nb, Mo, Hf, Ta, and W) Heusler compounds were systematically investigated by first-principles calculations. The main results are summarized as follows:

(1) Within the scope of Heusler structures, Ni_2MnT compounds with early transition metal atoms (T = Sc, Ti, Y, Zr, Nb, Hf, and Ta) were relatively stable in the Cu_2MnAl-type structure, which is consistent with the conventional atomic preferential occupation rule in the Heusler family. In contrast, Ni_2MnT compounds with late transition metal atoms (T = V, Cr, Mo, and W) preferred the Hg_2CuTi-type structure. For transition metal atoms lying in the same period in the periodic table, lattice parameters of Ni_2MnT decreased with the increase of valence electrons. Different from p-d covalent hybridization-dominated conventional Heusler compounds, the atomic radius was the determining factor for the lattice size in d-d metal bonding-controlled all-d-metal Heusler compounds.

(2) Owing to the strong coupling among lower tetragonal shear elastic constant C', higher Zener anisotropy factor A, deeply softened TA phonon modes, and typical peak structures in DOS below the Fermi level, the most likely martensitic phase transition can be expected in weakly magnetic Ni_2MnT compounds with late transition metal atoms (T = V, Cr, Mo, and W). Practically by applying hydrostatic pressure or imposing chemical pressure via adjusting the composition of Ti in the off-stoichiometric Ni-Mn-Ti system, magnetism got weakened, and the suppressed martensitic phase transition was re-evoked.

(3) Compared with p-d covalent hybridization-dominant conventional Heusler compounds, in representative all-d-metal Heusler compounds Ni_2MnY and Ni_2MnTa, nondirectional d-d metal bonding becomes prevailing. This fundamental transition was responsible for the enhancement of ductility and consequently helped in improving the fatigue life and service ability of all-d-metal Heusler compounds. Experimentally, it is speculated that low-energy d-d metal bonding can also benefit the nucleation and propagation of dislocations, which can further promote their ductile properties. Thus, tunable martensitic phase transition and improved ductility can enable all-d-metal Heuser compounds to be more promising and attractive as multiple functional magnetic materials.

(4) In this paper, we also reveal that experimentally observed antiferromagnetism in Ni_2MnTi originated from atomic diffusion process arrest during the transition from the high-temperature chemically disordered PM state to the low-temperature chemically and magnetically ordered ferromagnetic state, which resulted in the intermediate metastable and partially disordered antiferromagnetic phase.

It is believed that comprehensive and in-depth understanding of the mechanism of martensitic phase transition, improved ductility, and magnetism in all-d-metal Heusler compounds described in this paper can be helpful to explore martensitic phase transition materials with outstanding mechanical properties from both experimental and theoretical perspectives. Systematic exploration of this type of all-d-metal Heusler compounds is of importance in the context of promising solid-state cooling application based on the caloric effects of phase transition materials.

ACKNOWLEDGMENTS

This paper was supported by the special fund for introduced talent to initiate scientific research in Nanjing Tech University and National Natural Science Foundation of China (Grants No. 51831003 and No. 51771225). We are grateful to the High-Performance Computing Center of Nanjing Tech University for supporting the computational resources. Professor Levente Vitos and Dr. Wei Li are acknowledged for discussions on the EMTO-CPA method.

[1] F. Guillou, A. K. Pathak, D. Paudyal, Y. Mudryk, F. Wilhelm, A. Rogalev, and V. K. Pecharsky, Non-hysteretic first-order phase transition with large latent heat and giant low-field magnetocaloric effect, Nat. Commun. **9**, 2925 (2018).
[2] V. Franco, J. S. Blázquez, J. J. Ipus, J. Y. Law, L. M. Moreno-Ramírez, and A. Conde, Magnetocaloric effect: From materials research to refrigeration devices, Prog. Mater. Sci. **93**, 112 (2018).
[3] L. Manosa and A. Planes, Materials with giant mechanocaloric effects: Cooling by strength, Adv. Mater. **29**, 1603607 (2017).
[4] X. Moya, E. Defay, V. Heine, and N. D. Mathur, Too cool to work, Nat. Phys. **11**, 202 (2015).
[5] X. Moya, S. Kar-Narayan, and N. D. Mathur, Caloric materials near ferroic phase transitions, Nat. Mater. **13**, 439 (2014).
[6] Y. T. Song, X. Chen, V. Dabade, T. W. Shield, and R. D. James, Enhanced reversibility and unusual microstructure of a phase-transforming material, Nature (London) **502**, 85 (2013).
[7] T. Gottschall, A. Gràcia-Condal, M. Fries, A. Taubel, L. Pfeuffer, L. Mañosa, A. Planes, K. P. Skokov, and O. Gutfleisch, A multicaloric cooling cycle that exploits thermal hysteresis, Nat. Mater. **17**, 929 (2018).
[8] J. Liu, T. Gottschall, K. P. Skokov, J. D. Moore, and O. Gutfleisch, Giant magnetocaloric effect driven by structural transitions, Nat. Mater. **11**, 620 (2012).
[9] Z. Wu, Z. Liang, Y. Zhang, Z. Liu, J. Zhang, F. Motazedian, S. Bakhtiari, B. S. Shariat, Y. Liu, Y. Ren *et al.*, A eutectic dual-phase design towards superior mechanical properties of Heusler-type ferromagnetic shape memory alloys, Acta Mater. **181**, 278 (2019).
[10] Y. J. Huang, Q. D. Hu, J. Liu, L. Zeng, D. F. Zhang, and J. G. Li, Banded-like morphology and martensitic transformation of dual-phase Ni–Mn–In magnetic shape memory alloy with enhanced ductility, Acta Mater. **61**, 5702 (2013).
[11] D. Zhao, J. Liu, X. Chen, W. Sun, Y. Li, M. Zhang, Y. Shao, H. Zhang, and A. Yan, Giant caloric effect of low-hysteresis metamagnetic shape memory alloys with exceptional cyclic functionality, Acta Mater. **133**, 217 (2017).

[12] Z. Li, Z. Li, J. Yang, D. Li, B. Yang, H. Yan, Z. Nie, L. Hou, X. Li, Y. Zhang *et al.*, Large elastocaloric effect in a polycrystalline $Ni_{45.7}Co_{4.2}Mn_{37.3}Sb_{12.8}$ alloy with low transformation strain, Scr. Mater. **162**, 486 (2019).

[13] Q. Shen, D. Zhao, W. Sun, Y. Li, and J. Liu, The effect of Tb on elastocaloric and mechanical properties of Ni-Mn-In-Tb alloys, J. Alloys Compd. **696**, 538 (2017).

[14] W. Cai, L. Gao, A. L. Liu, J. H. Sui, and Z. Y. Gao, Martensitic transformation and mechanical properties of Ni–Mn–Ga–Y ferromagnetic shape memory alloys, Scr. Mater. **57**, 659 (2007).

[15] Z. Y. Wei, E. K. Liu, J. H. Chen, Y. Li, G. D. Liu, H. Z. Luo, X. K. Xi, H. W. Zhang, W. H. Wang, and G. H. Wu, Realization of multifunctional shape-memory ferromagnets in all-d-metal Heusler phases, Appl. Phys. Lett. **107**, 022406 (2015).

[16] Z. Y. Wei, E. K. Liu, Y. Li, X. L. Han, Z. W. Du, H. Z. Luo, G. D. Liu, X. K. Xi, H. W. Zhang, W. H. Wang *et al.*, Magnetostructural martensitic transformations with large volume changes and magneto-strains in all-d-metal Heusler alloys, Appl. Phys. Lett. **109**, 071904 (2016).

[17] V. G. de Paula and M. S. Reis, All-d-metal full Heusler alloys: A novel class of functional materials, Chem. Mater. **33**, 5483 (2021).

[18] D. Cong, W. Xiong, A. Planes, Y. Ren, L. Mañosa, P. Cao, Z. Nie, X. Sun, Z. Yang, X. Hong *et al.*, Colossal Elastocaloric Effect in Ferroelastic Ni-Mn-Ti Alloys, Phys. Rev. Lett. **122**, 255703 (2019).

[19] A. Aznar, A. Gracia-Conda, A. Planes, P. Lloveras, M. Barrio, J. L. Tamarit, W. X. Xiong, D. Y. Cong, C. Popescu, and L. Manosa, Giant barocaloric effect in all-d-metal Hensler shape memory alloys, Phys. Rev. Mater. **3**, 044406 (2019).

[20] Z. Wei, Y. Shen, Z. Zhang, J. Guo, B. Li, E. Liu, Z. Zhang, and J. Liu, Low-pressure-induced giant barocaloric effect in an all-d-metal Heusler $Ni_{35.5}Co_{14.5}Mn_{35}Ti_{15}$ magnetic shape memory alloy, APL Mater. **8**, 051101 (2020).

[21] Y. Shen, Z. Wei, W. Sun, Y. Zhang, E. Liu, and J. Liu, Large elastocaloric effect in directionally solidified all-d-metal Heusler metamagnetic shape memory alloys, Acta Mater. **188**, 677 (2020).

[22] H. N. Bez, A. K. Pathak, A. Biswas, N. Zarkevich, V. Balema, Y. Mudryk, D. D. Johnson, and V. K. Pecharsky, Giant enhancement of the magnetocaloric response in Ni-Co-Mn-Ti by rapid solidification, Acta Mater. **173**, 225 (2019).

[23] A. Taubel, B. Beckmann, L. Pfeuffer, N. Fortunato, F. Scheibel, S. Ener, T. Gottschall, K. P. Skokov, H. Zhang, and O. Gutfleisch, Tailoring magnetocaloric effect in all-d-metal Ni-Co-Mn-Ti Heusler alloys: A combined experimental and theoretical study, Acta Mater. **201**, 425 (2020).

[24] Y. Liu, A. Xiao, T. Yang, Z. Xu, X. Zhou, and T. Ma, Enhancing reversible entropy change of all-d-metal $Ni_{37.5}Co_{12.5}Mn_{35}Ti_{15}$ alloy by multiple external fields, Scr. Mater. **207**, 114303 (2022).

[25] See Supplemental Material at http://link.aps.org/supplemental/10.1103/PhysRevB.107.134440 for detailed comparison of multicaloric properties in Ni-Mn-Ti-based compounds with other materials for solid-state refrigeration, ELF distributions of Ni_2MnGa and isostructural Ni_2MnTi on (110) plane of unit cell in Cu_2MnAl-type structure, and lattice constant dependence of tetragonal shear elastic constant in stoichiometric Ni_2MnTi and off-stoichiometric $Ni_2Mn_{1+x}Ti_{1-x}$.

[26] W. Sun, J. Liu, B. Lu, Y. Li, and A. Yan, Large elastocaloric effect at small transformation strain in $Ni_{45}Mn_{44}Sn_{11}$ metamagnetic shape memory alloys, Scr. Mater. **114**, 1 (2016).

[27] Y. Li, W. Sun, D. Zhao, H. Xu, and J. Liu, An 8K elastocaloric temperature change induced by 1.3% transformation strain in $Ni_{44}Mn_{45-x}Sn_{11}Cu_x$ alloys, Scr. Mater. **130**, 278 (2017).

[28] L. Wei, X. Zhang, J. Liu, and L. Geng, Orientation dependent cyclic stability of the elastocaloric effect in textured Ni-Mn-Ga alloys, AIP Advances **8**, 055312 (2018).

[29] D. Zhao, J. Liu, Y. Feng, W. Sun, and A. Yan, Giant elastocaloric effect and its irreversibility in [001]-oriented $Ni_{45}Mn_{36.5}In_{13.5}Co_5$ meta-magnetic shape memory alloys, Appl. Phys. Lett. **110**, 021906 (2017).

[30] X.-M. Huang, L.-D. Wang, H.-X. Liu, H.-L. Yan, N. Jia, B. Yang, Z.-B. Li, Y.-D. Zhang, C. Esling, X. Zhao *et al.*, Correlation between microstructure and martensitic transformation, mechanical properties and elastocaloric effect in Ni-Mn-based alloys, Intermetallics **113**, 106579 (2019).

[31] D. Zhao, T. Castán, A. Planes, Z. Li, W. Sun, and J. Liu, Enhanced caloric effect induced by magnetoelastic coupling in NiMnGaCu Heusler alloys: Experimental study and theoretical analysis, Phys. Rev. B **96**, 224105 (2017).

[32] X. J. He, K. Xu, S. X. Wei, Y. L. Zhang, Z. Li, and C. Jing, Barocaloric effect associated with magneto-structural transformation studied by an effectively indirect method for the $Ni_{58.3}Mn_{17.1}Ga_{24.6}$ Heusler alloy, J. Mater. Sci. **52**, 2915 (2017).

[33] X. He, S. Wei, Y. Kang, Y. Zhang, Y. Cao, K. Xu, Z. Li, and C. Jing, Enhanced barocaloric effect produced by hydrostatic pressure-induced martensitic transformation for $Ni_{44.6}Co_{5.5}Mn_{35.5}In_{14.4}$ Heusler alloy, Scr. Mater. **145**, 58 (2018).

[34] X. He, Y. Kang, S. Wei, Y. Zhang, Y. Cao, K. Xu, Z. Li, C. Jing, and Z. Li, A large barocaloric effect and its reversible behavior with an enhanced relative volume change for $Ni_{42.3}Co_{7.9}Mn_{38.8}Sn_{11}$ Heusler alloy, J. Alloys Compd. **741**, 821 (2018).

[35] H. Liu, Z. Li, Y. Zhang, Z. Ni, K. Xu, and Y. Liu, A large barocaloric effect associated with paramagnetic martensitic transformation in $Co_{50}Fe_{2.5}V_{31.5}Ga_{16}$ quaternary Heusler alloy, Scr. Mater. **177**, 1 (2020).

[36] L. Mañosa, D. González-Alonso, A. Planes, E. Bonnot, M. Barrio, J.-L. Tamarit, S. Aksoy, and M. Acet, Giant solid-state barocaloric effect in the Ni-Mn-In magnetic shape-memory alloy, Nat. Mater. **9**, 478 (2010).

[37] A. Planes, E. Stern-Taulats, T. Castán, E. Vives, L. Mañosa, and A. Saxena, Caloric and multicaloric effects in shape memory alloys, Mater. Today: Proc. **2**, S477 (2015).

[38] N. H. Dung, Z. Q. Ou, L. Caron, L. Zhang, D. T. C. Thanh, G. A. de Wijs, R. A. de Groot, K. H. J. Buschow, and E. Brück, Mixed magnetism for refrigeration and energy conversion, Adv. Energy Mater. **1**, 1215 (2011).

[39] A. Fujita, S. Fujieda, Y. Hasegawa, and K. Fukamichi, Itinerant-electron metamagnetic transition and large magnetocaloric effects in $La(Fe_xSi_{1-x})_{13}$ compounds and their hydrides, Phys. Rev. B **67**, 104416 (2003).

[40] V. K. Pecharsky and J. K. A. Gschneidner, Giant Magnetocaloric Effect in $Gd_5(Si_2Ge_2)$, Phys. Rev. Lett. **78**, 4494 (1997).

[41] H. Wada and Y. Tanabe, Giant magnetocaloric effect of $MnAs_{1-x}Sb_x$, Appl. Phys. Lett. **79**, 3302 (2001).

[42] L. Huang, D. Y. Cong, H. L. Suo, and Y. D. Wang, Giant magnetic refrigeration capacity near room temperature in $Ni_{40}Co_{10}Mn_{40}Sn_{10}$ multifunctional alloy, Appl. Phys. Lett. **104**, 132407 (2014).

[43] O. Tegus, E. Bruck, K. H. J. Buschow, and F. R. de Boer, Transition-metal-based magnetic refrigerants for room-temperature applications, Nature (London) **415**, 150 (2002).

[44] S. A. Nikitin, G. Myalikgulyev, A. M. Tishin, M. P. Annaorazov, K. A. Asatryan, and A. L. Tyurin, The magnetocaloric effect in $Fe_{49}Rh_{51}$ compound, Phys. Lett. A **148**, 363 (1990).

[45] S. Stadler, M. Khan, J. Mitchell, N. Ali, A. M. Gomes, I. Dubenko, A. Y. Takeuchi, and A. P. Guimarães, Magnetocaloric properties of $Ni_2Mn_{1-x}Cu_xGa$, Appl. Phys. Lett. **88**, 192511 (2006).

[46] J. Tušek, K. Engelbrecht, R. Millán-Solsona, L. Mañosa, E. Vives, L. P. Mikkelsen, and N. Pryds, The elastocaloric effect: A way to cool efficiently, Adv. Energy Mater. **5**, 1500361 (2015).

[47] H. Ossmer, F. Lambrecht, M. Gültig, C. Chluba, E. Quandt, and M. Kohl, Evolution of temperature profiles in TiNi films for elastocaloric cooling, Acta Mater. **81**, 9 (2014).

[48] G. J. Pataky, E. Ertekin, and H. Sehitoglu, Elastocaloric cooling potential of NiTi, Ni_2FeGa, and CoNiAl, Acta Mater. **96**, 420 (2015).

[49] E. Bonnot, R. Romero, L. Mañosa, E. Vives, and A. Planes, Elastocaloric Effect Associated with the Martensitic Transition in Shape-Memory Alloys, Phys. Rev. Lett. **100**, 125901 (2008).

[50] F. Xiao, M. Jin, J. Liu, and X. Jin, Elastocaloric effect in $Ni_{50}Fe_{19}Ga_{27}Co_4$ single crystals, Acta Mater. **96**, 292 (2015).

[51] Z. Yang, D. Y. Cong, X. M. Sun, Z. H. Nie, and Y. D. Wang, Enhanced cyclability of elastocaloric effect in boron-microalloyed Ni-Mn-In magnetic shape memory alloys, Acta Mater. **127**, 33 (2017).

[52] S. Y. Dan'kov, A. M. Tishin, V. K. Pecharsky, and K. A. Gschneidner, Magnetic phase transitions and the magnetothermal properties of gadolinium, Phys. Rev. B **57**, 3478 (1998).

[53] K. Morrison, K. G. Sandeman, L. F. Cohen, C. P. Sasso, V. Basso, A. Barcza, M. Katter, J. D. Moore, K. P. Skokov, and O. Gutfleisch, Evaluation of the reliability of the measurement of key magnetocaloric properties: A round robin study of La(Fe, Si, Mn)H_δ conducted by the SSEEC consortium of European laboratories, Int. J. Refrig. **35**, 1528 (2012).

[54] F. Guillou, G. Porcari, H. Yibole, N. van Dijk, and E. Brück, Taming the first-order transition in giant magnetocaloric materials, Adv. Mater. **26**, 2671 (2014).

[55] L. Huang, D. Y. Cong, L. Ma, Z. H. Nie, Z. L. Wang, H. L. Suo, Y. Ren, and Y. D. Wang, Large reversible magnetocaloric effect in a Ni-Co-Mn-In magnetic shape memory alloy, Appl. Phys. Lett. **108**, 032405 (2016).

[56] T. Gottschall, K. P. Skokov, B. Frincu, and O. Gutfleisch, Large reversible magnetocaloric effect in Ni-Mn-In-Co, Appl. Phys. Lett. **106**, 021901 (2015).

[57] P. D. Thacher, Electrocaloric effects in some ferroelectric and antiferroelectric Pb(Zr, Ti)O_3 compounds, J. Appl. Phys. **39**, 1996 (1968).

[58] S. Yuce, M. Barrio, B. Emre, E. Stern-Taulats, A. Planes, J.-L. Tamarit, Y. Mudryk, K. A. Gschneidner Jr., V. K. Pecharsky, and L. Mañosa, Barocaloric effect in the magnetocaloric prototype $Gd_5Si_2Ge_2$, Appl. Phys. Lett. **101**, 071906 (2012).

[59] P. Lloveras, E. Stern-Taulats, M. Barrio, J. L. Tamarit, S. Crossley, W. Li, V. Pomjakushin, A. Planes, L. Mañosa, N. D. Mathur *et al.*, Giant barocaloric effects at low pressure in ferrielectric ammonium sulphate, Nat. Commun. **6**, 8801 (2015).

[60] Z. Y. Wei, W. Sun, Q. Shen, Y. Shen, Y. F. Zhang, E. K. Liu, and J. Liu, Elastocaloric effect of all-d-metal Heusler NiMnTi(Co) magnetic shape memory alloys by digital image correlation and infrared thermography, Appl. Phys. Lett. **114**, 101903 (2019).

[61] H.-L. Yan, L.-D. Wang, H.-X. Liu, X.-M. Huang, N. Jia, Z.-B. Li, B. Yang, Y.-D. Zhang, C. Esling, X. Zhao *et al.*, Giant elastocaloric effect and exceptional mechanical properties in an all-d-metal Ni-Mn-Ti alloy: Experimental and *ab-initio* studies, Mater. Des. **184**, 108180 (2019).

[62] L. Vitos, *Computational Quantum Mechanics for Materials Engineers: The EMTO Method and Applications* (Springer-Verlag, London, 2007).

[63] L. Vitos, H. L. Skriver, B. Johansson, and J. Kollár, Application of the exact muffin-tin orbitals theory: The spherical cell approximation, Comput. Mater. Sci. **18**, 24 (2000).

[64] L. Vitos, Total-energy method based on the exact muffin-tin orbitals theory, Phys. Rev. B **64**, 014107 (2001).

[65] L. Vitos, I. A. Abrikosov, and B. Johansson, Anisotropic Lattice Distortions in Random Alloys from First-Principles Theory, Phys. Rev. Lett. **87**, 156401 (2001).

[66] S. Huang, H. Huang, W. Li, D. Kim, S. Lu, X. Q. Li, E. Holmstrom, S. K. Kwon, and L. Vitos, Twinning in metastable high-entropy alloys, Nat. Commun. **9**, 2381 (2018).

[67] H. Y. Chen, Y. D. Wang, Z. H. Nie, R. G. Li, D. Y. Cong, W. J. Liu, F. Ye, Y. Z. Liu, P. Y. Cao, F. Y. Tian *et al.*, Unprecedented non-hysteretic superelasticity of 001-oriented NiCoFeGa single crystals, Nat. Mater. **19**, 712 (2020).

[68] Z. Dong, W. Li, S. Schonecker, B. Jiang, and L. Vitos, Invariant plastic deformation mechanism in paramagnetic nickel-iron alloys, Proc. Natl. Acad. Sci. USA **118**, e2023181118 (2021).

[69] G. Li, W. Li, S. Schönecker, X. Li, E. K. Delczeg-Czirjak, Y. O. Kvashnin, O. Eriksson, B. Johansson, and L. Vitos, Kinetic arrest induced antiferromagnetic order in hexagonal $FeMnP_{0.75}Si_{0.25}$ alloy, Appl. Phys. Lett. **105**, 262405 (2014).

[70] G. Li, O. Eriksson, B. Johansson, and L. Vitos, Thermodynamic-state and kinetic-process dependent dual ferromagnetic states in high-Si content FeMn(PSi) alloys, J. Appl. Phys. **118**, 213903 (2015).

[71] C.-M. Li, Q.-M. Hu, R. Yang, B. Johansson, and L. Vitos, Interplay between temperature and composition effects on the martensitic transformation in $Ni_{2+x}Mn_{1-x}Ga$ alloys, Appl. Phys. Lett. **98**, 261903 (2011).

[72] Q. M. Hu, H. B. Luo, C. M. Li, L. Vitos, and R. Yang, Composition dependent elastic modulus and phase stability of Ni_2MnGa based ferromagnetic shape memory alloys, Sci. China Tech. Sci. **55**, 295 (2012).

[73] M. Zelený, A. Sozinov, L. Straka, T. Björkman, and R. M. Nieminen, First-principles study of Co- and Cu-doped Ni_2MnGa along the tetragonal deformation path, Phys. Rev. B **89**, 184103 (2014).
[74] J. Hubbard, The magnetism of iron, Phys. Rev. B **19**, 2626 (1979).
[75] B. L. Gyorffy, A. J. Pindor, J. Staunton, G. M. Stocks, and H. Winter, A first-principles theory of ferromagnetic phase transitions in metals, J. Phys. F: Met. Phys. **15**, 1337 (1985).
[76] D. Vanderbilt, Soft self-consistent pseudopotentials in a generalized eigenvalue formalism, Phys. Rev. B **41**, 7892 (1990).
[77] J. P. Perdew, K. Burke, and M. Ernzerhof, Generalized Gradient Approximation Made Simple, Phys. Rev. Lett. **77**, 3865 (1996).
[78] V. L. Moruzzi, J. F. Janak, and K. Schwarz, Calculated thermal properties of metals, Phys. Rev. B **37**, 790 (1988).
[79] M. Wu, F. Zhou, R. Khenata, M. Kuang, and X. Wang, Phase transition and electronic structures of all-d-metal Heusler-type X_2MnTi compounds (X = Pd, Pt, Ag, Au, Cu, and Ni), Front. Chem. **8**, 546947 (2020).
[80] Y. Han, M. Wu, Y. Feng, Z. Cheng, T. Lin, T. Yang, R. Khenata, and X. Wang, Competition between cubic and tetragonal phases in all-d-metal Heusler alloys, $X_{2-x}Mn_{1+x}V$ (X = Pd, Ni, Pt, Ag, Au, Ir, Co; $x = 1, 0$): A new potential direction of the Heusler family, IUCrJ **6**, 465 (2019).
[81] H.-L. Yan, Y. Zhao, H.-X. Liu, M.-J. Zhang, H.-F. Zhang, J. Bai, N. Jia, B. Yang, Z.-B. Li, Y.-D. Zhang *et al.*, *Ab-initio* revelation on the origins of Ti substitution for Ga, Mn and Ni on ferromagnetism, phase stability and elastic properties in Ni_2MnGa, J. Alloy Compd. **821**, 153481 (2020).
[82] J. G. Tan, Z. H. Liu, Y. J. Zhang, G. T. Li, H. G. Zhang, G. D. Liu, and X. Q. Ma, Site preference and tetragonal distortion of Heusler alloy Mn-Ni-V, Results Phys. **12**, 1182 (2019).
[83] T. J. Burch, T. Litrenta, and J. I. Budnick, Hyperfine Studies of Site Occupation in Ternary Systems, Phys. Rev. Lett. **33**, 421 (1974).
[84] J. Zhang, Y. Wang, C. Hua, S. Yang, Y. Liu, J. Luo, T. Liu, J. Nai, and X. Tao, Prediction of bipolar VSi_2As_4 and VGe_2As_4 monolayers with high Curie temperature and strong magnetocrystalline anisotropy, Phys. Rev. B **106**, 235401 (2022).
[85] F. Han, X. Yan, F. Li, H. Yu, W. Li, X. Zhong, A. Bergara, and G. Yang, Prediction of monolayer FeP_4 with intrinsic half-metal ferrimagnetism above room temperature, Phys. Rev. B **107**, 024414 (2023).
[86] P. J. Webster, K. R. A. Ziebeck, S. L. Town, and M. S. Peak, Magnetic order and phase transformation in Ni_2MnGa, Philos. Mag. B **49**, 295 (1984).
[87] G. J. Li, E. K. Liu, H. G. Zhang, J. F. Qian, H. W. Zhang, J. L. Chen, W. H. Wang, and G. H. Wu, Unusual lattice constant changes and tunable magnetic moment compensation in $Mn_{50-x}Co_{25}Ga_{25+x}$ alloys, Appl. Phys. Lett. **101**, 102402 (2012).
[88] G. J. Li, E. K. Liu, H. G. Zhang, Y. J. Zhang, G. Z. Xu, H. Z. Luo, H. W. Zhang, W. H. Wang, and G. H. Wu, Role of covalent hybridization in the martensitic structure and magnetic properties of shape-memory alloys: The case of $Ni_{50}Mn_{5+x}Ga_{35-x}Cu_{10}$, Appl. Phys. Lett. **102**, 062407 (2013).
[89] J. Worgull, E. Petti, and J. Trivisonno, Behavior of the elastic properties near an intermediate phase transition in Ni_2MnGa, Phys. Rev. B **54**, 15695 (1996).
[90] T. Roy, M. E. Gruner, P. Entel, and A. Chakrabarti, Effect of substitution on elastic stability, electronic structure and magnetic property of Ni-Mn based Heusler alloys: An *ab initio* comparison, J. Alloys Compd. **632**, 822 (2015).
[91] C. M. Li, H. B. Luo, Q. M. Hu, R. Yang, B. Johansson, and L. Vitos, Temperature dependence of elastic properties of $Ni_{2+x}Mn_{1-x}Ga$ and $Ni_2Mn(Ga_{1-x}Al_x)$ from first principles, Phys. Rev. B **84**, 174117 (2011).
[92] P. Cao, F. Tian, W. Li, L. Vitos, and Y. Wang, Ideal superelasticity in Ni-based Heusler alloys, Acta Mater. **210**, 116816 (2021).
[93] F. Mouhat and F. X. Coudert, Necessary and sufficient elastic stability conditions in various crystal systems, Phys. Rev. B **90**, 224104 (2014).
[94] X. Ren, and K. Otsuka, in *Shape Memory Materials*, edited by T. Saburi (Trans Tech Publications Ltd, Zurich-Uetikon, 2000), pp. 429.
[95] C.-M. Li, H.-B. Luo, Q.-M. Hu, R. Yang, B. Johansson, and L. Vitos, First-principles investigation of the composition dependent properties of $Ni_{2+x}Mn_{1-x}Ga$ shape-memory alloys, Phys. Rev. B **82**, 024201 (2010).
[96] H. B. Luo, C. M. Li, Q. M. Hu, R. Yang, B. Johansson, and L. Vitos, Theoretical investigation of the effects of composition and atomic disordering on the properties of $Ni_2Mn(Al_{1-x}Ga_x)$ alloy, Acta Mater. **59**, 971 (2011).
[97] S. M. Shapiro, G. Xu, G. Gu, J. Gardner, and R. W. Fonda, Lattice dynamics of the high-temperature shape-memory alloy Nb-Ru, Phys. Rev. B **73**, 214114 (2006).
[98] S. M. Shapiro, G. Xu, B. L. Winn, D. L. Schlagel, T. Lograsso, and R. Erwin, Anomalous phonon behavior in the high-temperature shape-memory alloy $Ti_{50}Pd_{50-x}Cr_x$, Phys. Rev. B **76**, 054305 (2007).
[99] T. E. Stenger and J. Trivisonno, Ultrasonic study of the two-step martensitic phase transformation in Ni_2MnGa, Phys. Rev. B **57**, 2735 (1998).
[100] O. Heczko, H. Seiner, P. Stoklasová, P. Sedlák, J. Sermeus, C. Glorieux, A. Backen, S. Fähler, and M. Landa, Temperature dependence of elastic properties in austenite and martensite of Ni-Mn-Ga epitaxial films, Acta Mater. **145**, 298 (2018).
[101] X. Moya, D. González-Alonso, L. Mañosa, A. Planes, V. O. Garlea, T. A. Lograsso, D. L. Schlagel, J. L. Zarestky, S. Aksoy, and M. Acet, Lattice dynamics in magnetic superelastic Ni-Mn-In alloys: Neutron scattering and ultrasonic experiments, Phys. Rev. B **79**, 214118 (2009).
[102] C. Bungaro, K. M. Rabe, and A. D. Corso, First-principles study of lattice instabilities in ferromagnetic Ni_2MnGa, Phys. Rev. B **68**, 134104 (2003).
[103] S. Ghosh and S. Ghosh, Role of composition, site ordering, and magnetic structure for the structural stability of off-stoichiometric Ni_2MnSb alloys with excess Ni and Mn, Phys. Rev. B **99**, 064112 (2019).
[104] A. Kundu, S. Ghosh, and S. Ghosh, Effect of Fe and Co substitution on the martensitic stability and the elastic, electronic, and magnetic properties of Mn_2NiGa: Insights from *ab initio* calculations, Phys. Rev. B **96**, 174107 (2017).
[105] S. Singh, I. Valencia-Jaime, O. Pavlic, and A. H. Romero, Elastic, mechanical, and thermodynamic properties of Bi-Sb binaries: Effect of spin-orbit coupling, Phys. Rev. B **97**, 054108 (2018).

[106] T. Yue, P. Sui, Y. Zhao, J. Ni, S. Meng, and Z. Dai, Theoretical prediction of mechanics, transport, and thermoelectric properties of full Heusler compounds Na_2KSb and X_2CsSb (X = K,Rb), Phys. Rev. B **105**, 184304 (2022).
[107] W. Voigt, Ueber die Beziehung zwischen den beiden Elasticitätsconstanten isotroper Körper, Ann. Phys. **274**, 573 (1889).
[108] A. Reuss, Berechnung der Fließgrenze von Mischkristallen auf Grund der Plastizitätsbedingung für Einkristalle, Z. Ang. Math. Mech. **9**, 49 (1929).
[109] R. Hill, The elastic behaviour of a crystalline aggregate, Proc. Phys. Soc. Sect. A **65**, 349 (1952).
[110] M. Kohl, A. Agarwal, V. A. Chernenko, M. Ohtsuka, and K. Seemann, Shape memory effect and magnetostriction in polycrystalline Ni-Mn-Ga thin film microactuators, Mater. Sci. Eng. A **438**, 940 (2006).
[111] S. O. Kart and T. Cagin, Elastic properties of Ni_2MnGa from first-principles calculations, J. Alloys Compd. **508**, 177 (2010).
[112] S. Singh, S. W. D'Souza, J. Nayak, L. Caron, E. Suard, S. Chadov, and C. Felser, Effect of platinum substitution on the structural and magnetic properties of Ni_2MnGa ferromagnetic shape memory alloy, Phys. Rev. B **93**, 134102 (2016).
[113] S. F. Pugh, Relations between the elastic moduli and the plastic properties of polycrystalline pure metals, Phil. Mag. **45**, 823 (1954).
[114] I. N. Frantsevich, F. F. Voronov, and S. A. Bokuta, *Elastic Constants and Elastic Moduli of Metals and Insulators Handbook* (Naukova Dumka, Kiev, 1983).
[115] G. Li, E. Liu, G. Liu, W. Wang, and G. Wu, Density functional theory investigation on lattice dynamics, elastic properties and origin of vanished magnetism in Heusler compounds CoMnVZ (Z = Al, Ga), Chin. Phys. B **30**, 83103 (2021).
[116] B. Silvi and A. Savin, Classification of chemical bonds based on topological analysis of electron localization functions, Nature (London) **371**, 683 (1994).
[117] S. H. Zhang, Q. Wang, Y. Kawazoe, and P. Jena, Three-dimensional metallic boron nitride, J. Am. Chem. Soc. **135**, 18216 (2013).
[118] E. K. Liu, W. H. Wang, L. Feng, W. Zhu, G. J. Li, J. L. Chen, H. W. Zhang, G. H. Wu, C. B. Jiang, H. B. Xu *et al.*, Stable magnetostructural coupling with tunable magnetoresponsive effects in hexagonal ferromagnets, Nat. Commun. **3**, 873 (2012).
[119] M. E. Fine, L. D. Brown, and H. L. Marcus, Elastic constants versus melting temperature in metals, Scr. Metallurgica **18**, 951 (1984).
[120] M. Sanati, R. C. Albers, T. Lookman, and A. Saxena, Elastic constants, phonon density of states, and thermal properties of UO_2, Phys. Rev. B **84**, 014116 (2011).
[121] A. N. Vasil'ev, V. D. Buchel'nikov, T. Takagi, V. V. Khovailo, and E. I. Estrin, Shape memory ferromagnets, Phys. Usp. **46**, 559 (2003).
[122] S. A. Khandy, I. Islam, D. C. Gupta, R. Khenata, and A. Laref, Lattice dynamics, mechanical stability and electronic structure of Fe-based Heusler semiconductors, Sci. Rep. **9**, 1475 (2019).
[123] A. Ayuela, J. Enkovaara, and R. M. Nieminen, *Ab initio* study of tetragonal variants in Ni_2MnGa alloy, J. Phys.: Condens. Matter **14**, 5325 (2002).
[124] S. R. Barman, S. Banik, and A. Chakrabarti, Structural and electronic properties of Ni_2MnGa, Phys. Rev. B **72**, 184410 (2005).
[125] M. Ye, A. Kimura, Y. Miura, M. Shirai, Y. T. Cui, K. Shimada, H. Namatame, M. Taniguchi, S. Ueda, K. Kobayashi *et al.*, Role of Electronic Structure in the Martensitic Phase Transition of $Ni_2Mn_{1+x}Sn_{1-x}$ Studied by Hard-X-Ray Photoelectron Spectroscopy and Ab Initio Calculation, Phys. Rev. Lett. **104**, 176401 (2010).
[126] C. P. Opeil, B. Mihaila, R. K. Schulze, L. Mañosa, A. Planes, W. L. Hults, R. A. Fisher, P. S. Riseborough, P. B. Littlewood, J. L. Smith *et al.*, Combined Experimental and Theoretical Investigation of the Premartensitic Transition in Ni_2MnGa, Phys. Rev. Lett. **100**, 165703 (2008).
[127] C.-M. Li, H.-B. Luo, Q.-M. Hu, R. Yang, B. Johansson, and L. Vitos, Site preference and elastic properties of Fe-, Co-, and Cu-doped Ni_2MnGa shape memory alloys from first principles, Phys. Rev. B **84**, 024206 (2011).
[128] P. Entel, V. D. Buchelnikov, V. V. Khovailo, A. T. Zayak, W. A. Adeagbo, M. E. Gruner, H. C. Herper, and E. F. Wassermann, Modelling the phase diagram of magnetic shape memory Heusler alloys, J. Phys. D: Appl. Phys. **39**, 865 (2006).
[129] S. V. Faleev, Y. Ferrante, J. Jeong, M. G. Samant, B. Jones, and S. S. P. Parkin, Origin of the Tetragonal Ground State of Heusler Compounds, Phys. Rev. Appl. **7**, 034022 (2017).
[130] J. Winterlik, S. Chadov, A. Gupta, V. Alijani, T. Gasi, K. Filsinger, B. Balke, G. H. Fecher, C. A. Jenkins, F. Casper *et al.*, Design scheme of new tetragonal Heusler compounds for spin-transfer torque applications and its experimental realization, Adv. Mater. **24**, 6283 (2012).
[131] J. C. Suits, Structural instability in new magnetic heusler compounds, Solid State Commun. **18**, 423 (1976).
[132] T. Graf, C. Felser, and S. S. P. Parkin, Simple rules for the understanding of Heusler compounds, Prog. Solid State Chem. **39**, 1 (2011).
[133] A. Zheludev, S. M. Shapiro, P. Wochner, and L. E. Tanner, Precursor effects and premartensitic transformation in Ni_2MnGa, Phys. Rev. B **54**, 15045 (1996).
[134] S. Ener, J. Neuhaus, W. Petry, R. Mole, K. Hradil, M. Siewert, M. E. Gruner, P. Entel, I. Titov, and M. Acet, Effect of temperature and compositional changes on the phonon properties of Ni-Mn-Ga shape memory alloys, Phys. Rev. B **86**, 144305 (2012).
[135] A. T. Zayak, P. Entel, K. M. Rabe, W. A. Adeagbo, and M. Acet, Anomalous vibrational effects in nonmagnetic and magnetic Heusler alloys, Phys. Rev. B **72**, 054113 (2005).
[136] S. Ağduk and G. Gökoğlu, Ab initio lattice dynamics of Ni_2MnX (X = Sn, Sb) magnetic shape memory alloys, J. Alloys Compd. **511**, 9 (2012).
[137] A. Landa, P. Söderlind, I. I. Naumov, J. E. Klepeis, and L. Vitos, Kohn anomaly and phase stability in group VB transition metals, Computation **6**, 29 (2018).
[138] G. Li, E. Liu, and G. Wu, *d*-*d* hybridization controlled large-volume-change martensitic phase transition in Ni-Mn-Ti-based all-*d*-metal Heusler compounds, J. Alloy Compd. **923**, 166369 (2022).
[139] R. Arróyave, A. Junkaew, A. Chivukula, S. Bajaj, C. Y. Yao, and A. Garay, Investigation of the structural stability of Co_2NiGa shape memory alloys via *ab initio* methods, Acta Mater. **58**, 5220 (2010).